Palaeogeography, Palaeoclimatology, Palaeoecology 371 (2013) 9–25

Contents lists available at SciVerse ScienceDirect

Palaeogeography, Palaeoclimatology, Palaeoecology

journal homepage: www.elsevier.com/locate/palaeo

Black shale formation during the Latest Danian Event and the Paleocene–Eocene Thermal Maximum in central Egypt: Two of a kind?

Peter Schulte [a,*], Lorenz Schwark [b], Peter Stassen [c], Tanja J. Kouwenhoven [c], André Bornemann [d], Robert P. Speijer [c]

[a] GeoZentrum Nordbayern, Universität Erlangen, D-91054 Erlangen, Germany
[b] Institut für Geowissenschaften, Christian-Albrechts Universität Kiel, Ludewig-Meyn-Str. 10, D-24118 Kiel, Germany
[c] Department of Earth and Environmental Sciences, K.U. Leuven, B-3001 Leuven, Belgium
[d] Institut für Geophysik und Geologie, Universität Leipzig, Talstraße 35, D-04103 Leipzig, Germany

ARTICLE INFO

Article history:
Received 31 March 2012
Received in revised form 28 October 2012
Accepted 27 November 2012
Available online 14 December 2012

Keywords:
Paleocene
Eocene
Egypt
Tethyan shelf
Hyperthermals
PETM
LDE

ABSTRACT

The Paleocene–Eocene Thermal Maximum (PETM; ~55.8 Ma) is considered as the most severe of a series of transient warming events ("hyperthermals") that occurred during the Early Paleogene. However, the extent and magnitude of environmental changes during the short-lived warming events pre- and post-dating the PETM are still poorly constrained. In this study, we focus on the Latest Danian Event (LDE, ~61.7 Ma) and compare it to the PETM. We present high-resolution micropaleontological, geochemical, and mineralogical data of the PETM and the LDE in two adjacent sections from the Gebel Qreiya area in Egypt. There, both events are characterized by a distinct set of event beds overlying an unconformity. They are associated with intense carbonate dissolution and substantial changes in the benthic foraminifera fauna. Moreover, both show an abrupt drop of siliciclastic input (sediment starvation) correlative to the onset of black shale formation and a strong enrichment in redox-sensitive trace elements. The evidence for enhanced detrital input during the onset of the PETM and a longer recovery phase with enhanced phosphorus-sedimentation during the PETM attests a stronger environmental impact of this event compared to the LDE.

According to Rock-Eval and elemental analysis, the PETM as well as the LDE event beds have up to 4 wt.% organic carbon, small amounts of volatile hydrocarbons, but high amounts of highly weathered and inert organic matter ("black carbon"). During pyrolysis, the extremely high temperatures for the maximum release of hydrocarbons of the PETM and LDE samples correspond to thermal heating of >170 °C, which is incompatible with the sediment burial history. Therefore, we suggest that the organic matter in both event deposits does not reflect well-preserved marine biomass but predominantly represents a mixture of heavily weathered autochthonous marine material and allochthonous combustion residues. Differences in preservation and/or type of organic matter are also likely to account for the divergent stable isotope anomalies of organic carbon: the well-known negative carbon isotope anomaly at the PETM and a positive anomaly at the LDE. Although warming, water column stratification, and enhanced nutrient input may have promoted anoxic conditions on the shelf during the LDE as well as during PETM, our results support rapid sea level rise and clastic starvation as one important mechanism for black shale formation and carbon sequestration for both events. This result underlines the similarity of both hyperthermal events in terms of environmental changes recorded on the Southern Tethyan margin, with the PETM showing an additional early phase of strong detrital input not revealed at the LDE.

1. Introduction

The early Paleogene greenhouse episode is punctuated by a series of transient warming events ("hyperthermals", Thomas and Zachos, 2000; Speijer, 2003; Bernaola et al., 2007; Nicolo et al., 2007; Quillévéré et al., 2008; Agnini et al., 2009; Bornemann et al., 2009). These hyperthermals generally show a negative carbon isotope excursion ("CIE") in marine environments, as well as enhanced sea-floor carbonate dissolution, deep- to intermediate water oxygen depletion, and pronounced (transient) changes in marine benthic faunas. These characteristics are indicative for the massive addition of ^{13}C-depleted carbon to the ocean–atmosphere system from an external carbon reservoir, leading to increasing atmospheric pCO_2 and temperature, substantial shoaling of the lysocline and calcite compensation depth (CCD), and accelerated hydrologic and weathering cycles (e.g., Zachos et al., 2005; Nicolo et al., 2007; Sluijs et al., 2007). The source and amount of the isotopically light carbon, however, are still debated (e.g., Higgins and Schrag, 2006). It may derive from the catastrophic release of gas hydrates (e.g., Dickens et al., 1995) or from large-scale venting triggered by magma intruding

* Corresponding author.
E-mail address: schulte@geol.uni-erlangen.de (P. Schulte).

0031-0182/$ – see front matter © 2012 Elsevier B.V. All rights reserved.
http://dx.doi.org/10.1016/j.palaeo.2012.11.027

organic-rich sediments (e.g., Svensen et al., 2004). Equally discussed is the mechanism (e.g., weathering or productivity increase) and rate by which the excess carbon was sequestered from the atmosphere and oceans (see Bains et al., 2000; Torfstein et al., 2009).

The most prominent and well-documented hyperthermal is the ~170 ky-long Paleocene–Eocene Thermal Maximum ("PETM", Fig. 1, ~55.8 Ma) that was associated with global warming of up to 10 °C and a major benthic foraminifera extinction event ("BFEE", Kennett and Stott, 1991; Thomas and Shackleton, 1996; Speijer et al., 2000; Zachos et al., 2001; Sluijs et al., 2007). Additionally proposed hyperthermals, albeit of shorter duration and lower magnitude, include (i) the early Danian Dan-C2 event (~65.2 Ma, Fig. 1, Quillévéré et al., 2008; Coccioni et al., 2010); (ii) the Latest Danian Event (~61.7 Ma, Fig. 1, Speijer, 2003; Bornemann et al., 2009); (iii) the Early-Late Paleocene Event (~58.2 Ma, Fig. 1, Bralower et al., 2002; Petrizzo, 2005; Bernaola et al., 2007), and (iv) the early Eocene Thermal Maxima 2 and 3 (~53.7 and ~53.6 Ma, respectively, Lourens et al., 2005; Nicolo et al., 2007; Agnini et al., 2009; Stap et al., 2009; Zachos et al., 2010). However, the stratigraphy and global signature of these suspected hyperthermal events pre- and post-dating the PETM are still poorly constrained, although their environmental consequences and rates of change may provide important clues to the carbon release and sequestration mechanisms.

Specifically, the Latest Danian Event (LDE) has been proposed as a transient warming event (Figs. 1 and 2). It was first recognized on the southern Tethyan margin (Egypt and Tunisia, Speijer, 2003; Guasti et al., 2006; Van Itterbeeck et al., 2007; Bornemann et al., 2009; Sprong et al., 2011, 2012), and subsequently observed in the eastern Atlantic (Zumaia, Arenillas et al., 2008), and in the Pacific (Westerhold et al., 2011) at the top of magnetochron C27n close to the planktic foraminiferal Subzone P3a/P3b boundary and within the calcareous nannofossil Zone NP4 (Steurbaut and Sztrákos, 2008; Sprong et al., 2009). Distinctive features of this event are an up to 2‰ negative carbon isotope excursion (Fig. 2, Arenillas et al., 2008; Bornemann et al., 2009; Westerhold et al., 2011), evidence for carbonate dissolution, benthic faunal changes, and sea-level changes (Speijer, 2003), as well as warming (Fig. 2, Westerhold et al., 2011). The total duration of the event has been estimated to be ~191 ky (Bornemann et al., 2009) or ~190 to 200 ky (Westerhold et al., 2011), with the latter period being very similar to the duration of the PETM as outlined above.

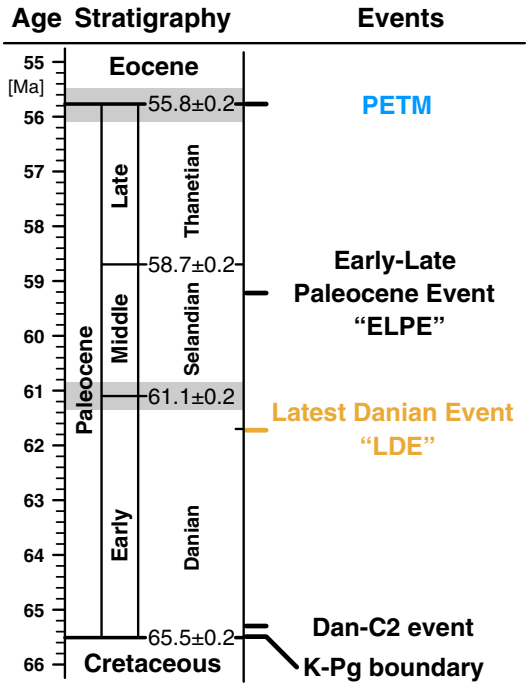

Fig. 1. Time scale of the Paleocene with important global events. Modified after Gradstein et al. (2004).

In this study, we investigate the LDE and PETM from the extensive outcrops of the Paleocene–Eocene succession at Gebel Qreiya in Central Egypt (Fig. 3). There, as well as in other Egyptian sections (e.g., Gebel Aweina, Gebel Nezzi; Fig. 3), the LDE has similar features as the PETM record in terms of lithological and biotic changes and both are correlated to a distinct set of event beds (Speijer and Wagner, 2002; Speijer, 2003). This provides an excellent opportunity to test the hypothesis that the LDE represents a hyperthermal event by comparing the signature of both the LDE and PETM event through a high-resolution, micropaleontological, mineralogical, and organic–inorganic geochemical study. Specifically, we aim to investigate the mechanisms of black shale formation that characterize both the LDE as well as the PETM event beds in Central Egypt (Speijer and Wagner, 2002; Speijer, 2003). A lowering of oxygen availability, commonly associated with black shale formation, has been recorded during the PETM at several deep marine sites (Bralower et al., 1997; Chun et al., 2010; Nicolo et al., 2010) and in shelf sections (Speijer et al., 1997; Speijer and Wagner, 2002; Gavrilov et al., 2003). Oxygen depletion controlled benthic faunal changes (e.g., the BFEE at the PETM) but may also triggered an increased carbon preservation and burial, which may have acted as a feedback mechanism for excess carbon sequestration during the recovery phase of these transient warming events (e.g., Speijer and Wagner, 2002).

2. Materials and methods

2.1. The Gebel Qreiya sections

The sections studied are located in the Eastern Desert, close to the Nile Valley at Gebel Qreiya (Fig. 3). The Qreiya 2 and 3 sections are situated east of the southern entrance of Wadi Qena, about 50 km north-east of Qena City. The Q3 LDE section is in the eastern end of Gebel Qreiya (26°N 27.702', 33°E 1.905'; altitude 380 m a.s.l., Sprong et al., 2011). The Q2 PETM section is located on the southeastern nose of Gebel Qreiya (26°N 27.192', 33°E 2.233'; altitude 437 m a.s.l.), about 1000 m southeast of Q3.

In the Qreiya 3 section, the LDE beds are intercalated within the marls of the Dakhla Formation close to the P3a–P3b planktonic foraminiferal subzonal boundary (Fig. 4, Sprong et al., 2009). The uppermost 15 cm of the marls below the event deposit are dark grey, contain few fish remains, and are bioturbated at the top. The lower contact of the LDE deposit with the Dakhla Formation is undulatory and possibly erosive (Sprong et al., 2009). The LDE deposit consists of two distinct beds (1 and 2). Bed 1 (8.2 to 8.3 m) is a dark purplish-brown, organic-rich laminated marl containing fish remains, P-nodules and abundant planktonic foraminifers. The upper 7 cm of bed 1 contains dark grey clay lenses parallel to the lamination. These represent downward penetrating bioturbations from bed 2 (8.3 to 8.45 m), which is dark grey marly shale and contains hematitic or limonitic bivalve and gastropod moulds. Grey shaley marls conformably overlie the LDE beds. About 10 m south of the Q3 section, a several-meter wide and ~20 cm thick calcarenite channel fill is present and cuts into the LDE beds. The channel fill shows upward-fining and is extremely rich in planktic and benthic foraminifera.

In the Qreiya 2 PETM section, the "Dababiya Quarry Beds" (hereafter PETM beds) that characterize the PETM event in Central Egypt (Dupuis et al., 2003) are intercalated within the lower part of the Esna Formation, overlying the Esna 1 unit (Knox et al., 2003; Ouda, 2003). The base of the PETM beds correlates with the BFEE and to the P5a/E1 foraminiferal subzone delineating the base of the Eocene (Fig. 4, Dupuis et al., 2003; Berggren and Pearson, 2005; Aubry et al., 2007). Above the P-E boundary, five PETM beds can be distinguished lithologically: Bed 1 (7.9 to 8.1 m): dark grey, non-calcareous laminated shale with few P-nodules in its upper centimeters. Bed 2 (8.1 to 8.3 m): brown to dark grey, laminated shale with some fish remains and P-nodules. The

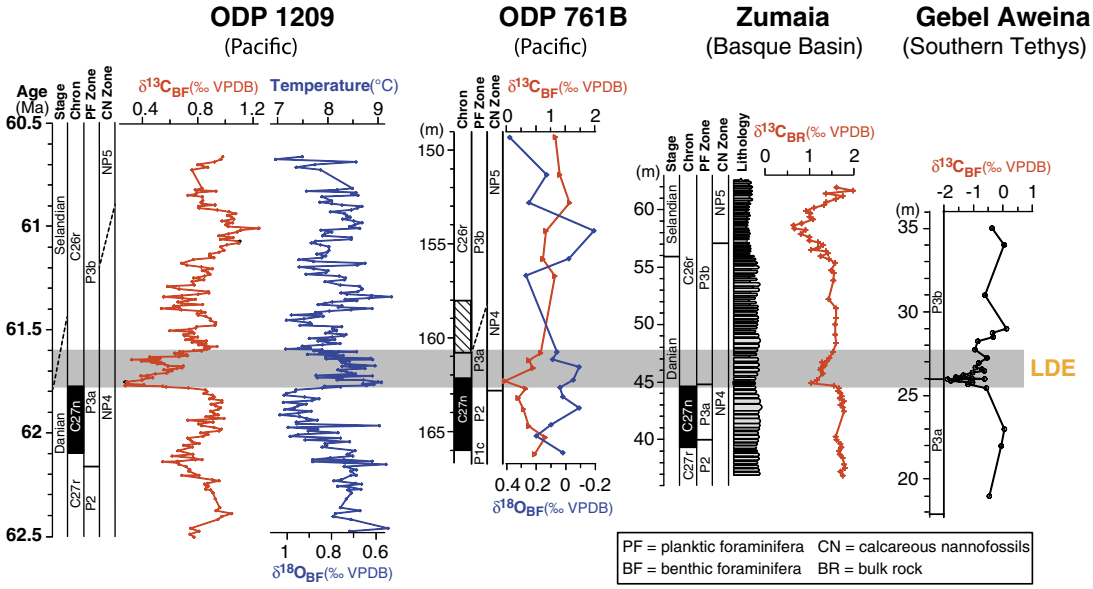

Fig. 2. Stable isotope chemostratigraphy across the latest Danian.
Compiled from Bornemann et al. (2009) and Westerhold et al. (2011).

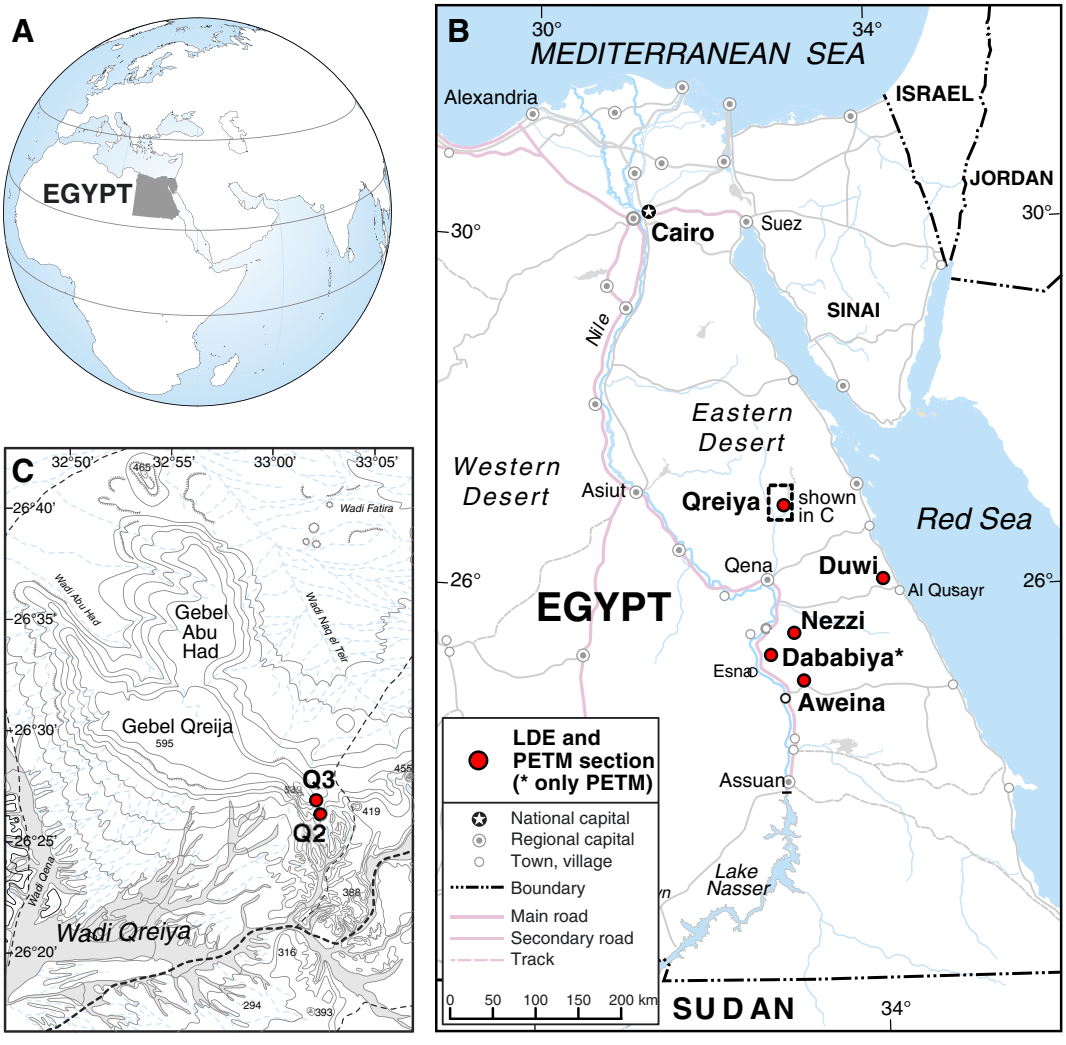

Fig. 3. (A) Global map. (B) Map of Egypt with sections that include the LDE and/or the PETM. (C) Map of the Gebel Qreiya region with the studied sections Q2 PETM and Q3 LDE.

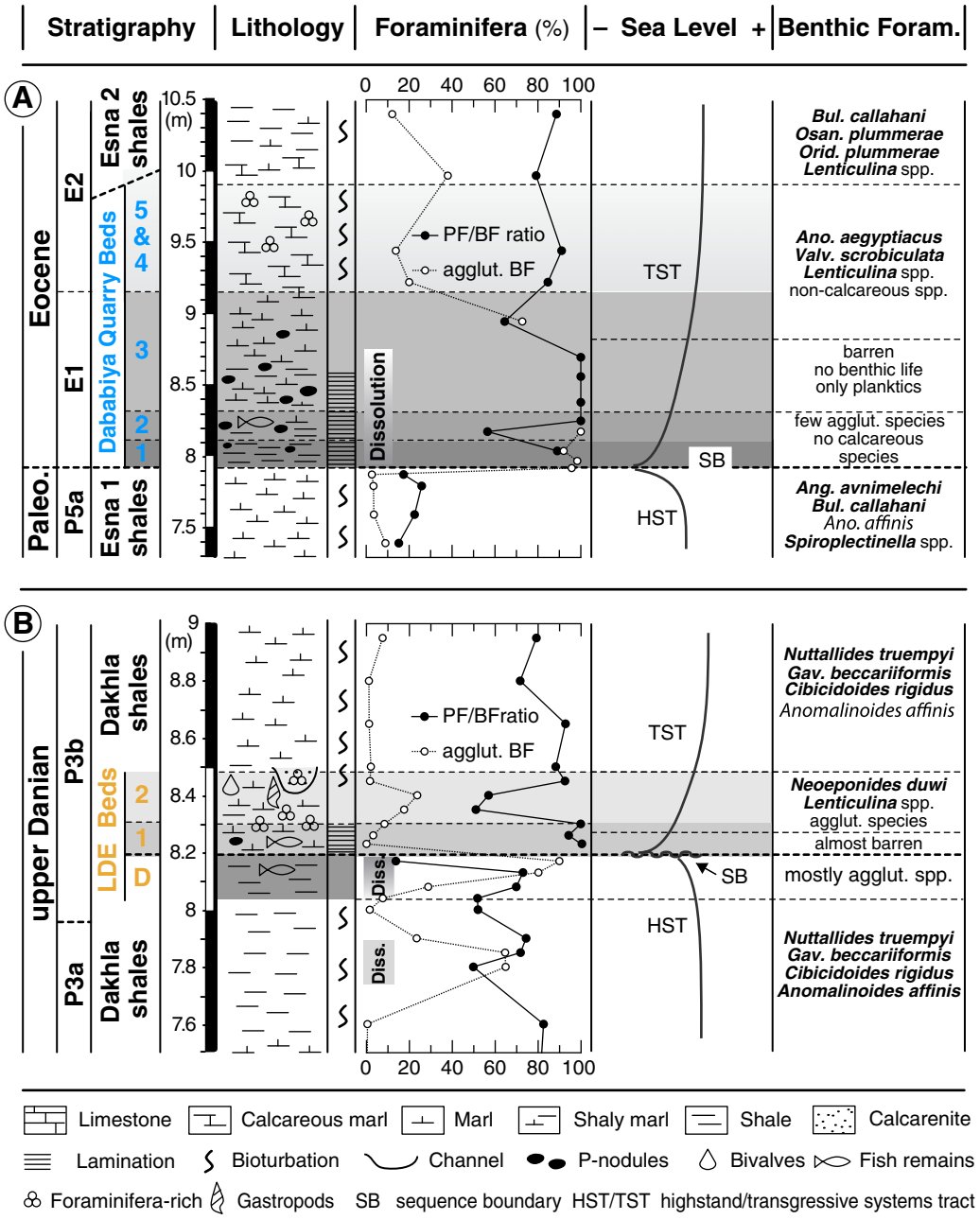

Fig. 4. Lithological columns of the (A) Q2 PETM and the (B) Q3 LDE section with planktic/benthic (PF/BF) foraminifera ratios, estimated sea-level fluctuations, and the relative amount of agglutinated benthic foraminifera. Note the 50% scale change between the more expanded PETM vs. the thinner LDE event beds.

shale is mostly non-calcareous except for the uppermost 4 centimeters. Bed 3 (8.3 to 9.15 m): dark brown to grey, moderately to highly calcareous marl. The lower 30 cm of this bed show a distinct lamination, whereas the upper part is not laminated. P-nodules are present throughout this unit and some fish remains have been observed in the lower part. Beds 4 and 5, as distinguished by Knox et al. (2003), are difficult to separate in this section and are therefore combined (9.15 to 10 m): medium pale to light grey, calcareous marls with lenses and mm-thin layers of silt-sized foraminifera. A distinct calcarenite bed, as observed in other PETM sections in Egypt within bed 5 has not been observed. Above the PETM beds, the Esna 2 unit continues as dark clayey marl.

2.2. Sample preparation

Detailed methods for the foraminifera analyses are outlined in Ernst et al. (2006) and Sprong et al. (2011). For mineralogical and element geochemical analysis, samples were ground to a grain size <10 μm with a McCrone Micromill (Srodon et al., 2001).

2.3. Mineralogical analysis

The mineralogical composition of the powdered samples was determined at the University of Erlangen using a Siemens D5000 X-ray diffractometer. This instrument is fitted with a copper tube (CuKα = 1.54178 Å), operating at 40 kV and 35 mA, and a post-diffraction graphite monochromator. Samples were side loaded into a holder for random orientation and scanned from 5° to 65° 2Θ in steps of 0.02° and 4 s scanning time. For clay mineralogy, the decalcified <2 μm fraction was saturated with MgCl, sucked through a ceramic filter, and analyzed as air-dried, glycolated, and heated (450 °C for 1 h) specimens before X-ray analysis from 3 to 36 °2Θ in steps of 0.02° at 2 s per step.

The BGMN 5.0.12 Rietveld refinement program (Bergmann et al., 1998) was used for mineral quantification and provided very good fits: (i) the observed weighted residual errors R_{wp} ranged from ~8.5 to ~12.5%, (ii) the weighted residual errors R_{wp} approach the statistically expected values R_{exp}, indicating good agreement between the observed and simulated XRD patterns, and (iii) the calculated quality parameter 1- ρ ranged from excellent values as low as 1.3 to higher values of ~3.5%. Higher values of 1-ρ are confined to the PETM Bed 1 and are probably related to compositional changes in the smectite mineralogy that were not considered in the present study. To address precision of the XRD analysis, multiple preparations and subsequent analysis of a single sample were conducted, resulting in an interquartile range of the major mineral phases in the acceptable range of about 0.5 to 1 wt.%. The accuracy of the Rietveld refinement was tested by several representative samples spiked with 10 wt.% zincite (ZnS) as an internal standard. This standard could be recovered satisfactorily by all refinements, although a tendency towards higher values is obvious (~11 to ~14 wt.% recovery). These overestimations are mostly related to the presence of additional X-ray amorphous components including organic material.

2.4. Geochemical analysis

For major element analyses, glass disks were processed by melting about 1 g of ground bulk sediment with a Li-tetraborate flux and analyzed at the University of Erlangen with a PHILIPS PW 2400 sequential wavelength dispersive X-ray spectrometer. Analytical precision was verified by the preparation and analysis of several in-house standards. Relative precision and accuracy were found to be better than 4 rel% for all major elements, except for P (better than 8 rel%). The trace element concentrations of Ni, Cr, Cu, Co, Zn, As, Rb, Sr, Zr, Pb, Th, and U were determined from powdered samples at the University of Heidelberg with the energy-dispersive miniprobe multi-element analyzer (see Cheburkin and Shotyk, 1996). The trace elements have an average detection limit of 2 to 3 ppm. Analytical accuracy (about 5 rel% for trace elements) was checked by analyzing several international standards and precision was determined by replicate analyses of several samples.

For stable isotopes of organic carbon and for TOC analysis, carbonate was removed from the ground samples with hot 10% HCl. Subsequently, the absence of carbonates was checked by XRD. CO_2 for the stable isotope analysis was prepared by sealed-tube combustion and isotopic abundances were measured in a Finnigan MAT 252 mass spectrometer at University of Erlangen on cryogenically purified CO_2. Accuracy and precision were checked by replicate analyses of the graphite standard USGS 24 as well as by replicate analysis of critical samples. Precision was better than ±0.1‰ (1σ). The decalcified samples were also used for elemental analysis. Concentrations of total organic carbon (TOC) were determined by using a VARIO EL elemental analyzer (Elementar). Pyrolysis was performed using a ROCK-EVAL II-PLUS analyzer (Vinci Technologies) following standardized procedures (see Lüniger and Schwark, 2002).

3. Results and interpretation

3.1. Benthic foraminifera assemblages

The Q3 LDE event beds show distinct changes in benthic foraminiferal assemblages (Fig. 4B) which were used to reconstruct the pealeo-waterdepth by using the depth-ranges of the benthic formaminifera species shown in Table 1.

The Dahkla shales below the LDE are dominated by outer neritic to upper bathyal species (e.g., *Cibicidoides rigidus*, *Anomalinoides affinis*), and contain up to 25% of species with a bathyal preference (*Nuttallides truempyi*, *Gavelinella beccariiformis*; c.f. Table 1). The paleo-water depth estimate for this stratigraphic interval is between ~150 and 250 m (Speijer, 2003; Sprong et al., 2011). About 70 cm below the LDE, from 7.5 m upwards, *G. beccariiformis* is no longer present in the assemblages. Two thin intervals below the LDE (7.8 to 8 m and 8.05 to 8.2 m) show an increase in non-calcareous benthic foraminifera (up to 80%), and a drop in planktic and benthic foraminifera numbers, which, together with a $CaCO_3$ content of <3 wt.% indicates severe carbonate dissolution (Fig. 4B; Sprong et al., 2011). Between these dissolution levels, at ~8 m, the bathyal foraminifera are absent, indicating 50 m or less shallowing to outer neritic paleodepths before the LDE. In LDE bed I the absence of in-situ benthic foraminifera is probably associated with severe oxygen deprivation at the sea floor; in agreement with sedimentologic and geochemical evidence for anoxia outlined in the following, and with the high planktic-benthic ratios (90 to 99%, Fig. 4B, Sprong et al., 2011). The high numbers of planktic foraminifera in the upper part of bed 1 (>8000 species per g sediment) support either high surface productivity or a period of condensation and winnowing during the LDE. During deposition of LDE bed 2, sea-floor oxygenation improves, and opportunistic inner-middle neritic taxa occur, such as *Neoeponides duwi*, *Siphogenerinoides esnehensis* and costate *Lenticulina* spp. This *N. duwi* assemblage suggests a significantly shallower paleodepth of ~50 m However, similar influxes of shallow-water taxa including dominant *N. duwi* were recorded before at several locations (e.g., Speijer, 2003), and attributed to recolonization. Similarly, Sprong et al. (2011) argue that the influx at Q3 cannot be interpreted in terms of absolute paleodepth, but instead, indicates repopulation of niches vacated during the anoxic event of LDE bed I. Above the LDE deposit, the outer neritic taxa are the first to replace the *N. duwi* assemblage. Eventually the outer neritic-bathyal benthic fauna that dominated before the LDE is completely restored, indicating that pre-LDE conditions are re-established. No benthic extinctions are recorded across the LDE.

In the Q2 PETM section, three main benthic foraminiferal assemblages can be observed across the PETM, very similar to the Dababiya PETM section (Ernst et al., 2006). The latest Paleocene assemblage is characterized by abundant outer neritic to bathyal taxa (e.g., *Angulogavelinella avnimelechi*, *Bulimina callahani*, *Anomalinoides affinis*, and *Spiroplectinella* spp.), indicating paleo-water depth of ~200 m (c.f. Table 1); the high amount of endobenthic species pointing to lower oxygen levels. The low foraminiferal numbers and a P/B ratio too low for an outer neritic environment (Fig. 4) suggest selective post-mortem dissolution of planktic foraminifera without significantly affecting the calcareous benthic foraminiferal assemblages. Latest Paleocene mesotrophic environmental conditions ended abruptly with the extinction of *A. avnimelechi* and changed into eutrophic and anoxic bottom conditions during the early part of the PETM. The base of PETM bed 1 contains some non-calcareous agglutinated taxa and is likely the result of post-mortem dissolution of (reworked?) benthic assemblages during the early stages of

Table 1
Benthic foraminifera key species used for paleodepth reconstructions. For detailed information see Speijer and Wagner (2002), Speijer (2003), Ernst et al. (2006), Sprong et al. (2011, 2012).

Benthic foraminifera taxon	Depth range
Angulogavelinella avnimelechi	ON–UB[a]
Anomalinoides aegyptiacus	IN–MN[b]
Anomalinoides affinis	ON–UB
Bulimina callahani	ON–UB
Cibicidoides rigidus	ON–UB
Gavelinella beccariiformis	UB[a]
Neoeponides duwi	IN–MN[b]
Nuttallides truempyi	UB
Lenticulina spp.	IN–MN (ON)
Lenticulina spp. (costate)	IN–MN[b]
Siphogenerinoides esnehensis	IN–MN[b]
Spiroplectinella spp.	ON–UB
Valvulineria scrobiculata	IN–MN[b]

IN/MN/ON: inner/middle/outer neritic; UB: upper bathyal.
[a] Extinct at BFEE.
[b] Taxa with inferred wider depth range.

the PETM. The absence of benthic foraminifera as well as sediment lamination in beds 1 to 3 suggest that anoxia inhibited the establishment of benthic life. From the middle part of bed 3 upsection, oxygenation improved slightly enabling recolonization by a benthic fauna with shallow water affinity (Speijer et al., 1997; Speijer and Wagner, 2002): *Anomalinoides aegyptiacus*, *Valvulineria scrobiculata*, *Lenticulina* spp. and non-calcareous species. Finally, the Eocene benthic foraminiferal assemblage of the overlying Esna 2 shales resembles the latest Paleocene fauna (Fig. 4), with the exception of taxa that had gone extinct, such as *A. avnimelechi* and *G. beccariiformis*. The decline of opportunistic species and reappearance of outer neritic species indicate further improved environmental conditions and the return to pre-PETM conditions.

3.2. Bulk rock and clay mineralogy

Across the LDE as well as the PETM beds, the XRD data reveal strong changes in abundance and composition of mineral assemblages (Figs. 5 and 6). In part, these changes reflect absence of dilution by calcite within dissolution intervals (e.g., within PETM bed 1) or increased dilution due to a strong increase in the calcite content (e.g., within the LDE beds and the PETM beds 2 and 3). However, across the PETM beds, there is also a marked increase in siliciclastic detritus compared to the enclosing shales (Fig. 6). Specifically, the PETM bed 1 reveals a dramatic increase of quartz, feldspar, and phyllosilicates. Moreover, this increase corresponds to a prominent change from an illite-smectite- to a pure smectite-dominated assemblage and an increase of clay minerals relative to the quartz content. The smectite may derive from the erosion of soils, drained lowlands, or altered volcanic deposits (e.g., Curtis, 1990; Bengtsson and Stevens, 1998). Such a change has not been observed at the Q3 LDE section, which shows a consistent kaolinite-dominated mineralogy. The decrease in the relative amount of phyllosilicates observed at the base of the LDE beds is rather the effect of rapid reproduction of foraminifera shells in surface waters and the resulting dilution of the siliciclastic detritus. Likewise condensation during a rapid sea-level rise could explain the drop in siliciclastic input, while winnowing due to enhanced current activity is not consistent with the prevalence of anoxic conditions during deposition of the foraminifera-rich bed.

Another important characteristic is high abundances of anhydrite (>15 wt.%) in the PETM and LDE event beds, although anhydrite veins were avoided during sampling. Therefore, a decent amount of finely-disseminated anhydrite or very thin anhydrite veins is present within the shales. A primary origin of the anhydite is very unlikely as shown by anhydrite veins crosscutting bedding and by fossil assemblages excluding hypersalinity. In the LDE beds, the anhydrite enrichment is associated with very high amounts of iron-oxides (up to 10 wt.%), whereas the PETM beds show only a minor increase of these iron minerals. Such a high anhydrite and iron-hydroxide content is usually indicative of intensive pyrite oxidation during weathering, in agreement with the rather low amounts of pyrite in the LDE and PETM beds (<0.3 wt.%) compared to non-weathered black shales (e.g., Littke et al., 1991; van Os et al., 1995). This would also explain at least part of the dissolution phenomena observed in the foraminiferal assemblages in various parts of the PETM and LDE sequences.

3.3. Detritus-sensitive trace elements

The major element trends reflect mainly the mineralogical changes outlined above, thus we focus on element/Al ratios to reveal changes in the character of the detrital material as shown in Fig. 7. In the background sediments of the Esna and Dakhla shales, the Si/Al ratio is relatively stable. The lower Si/Al ratios of the Dakhla shales in the LDE section are explained by the lower quartz content and the dominance

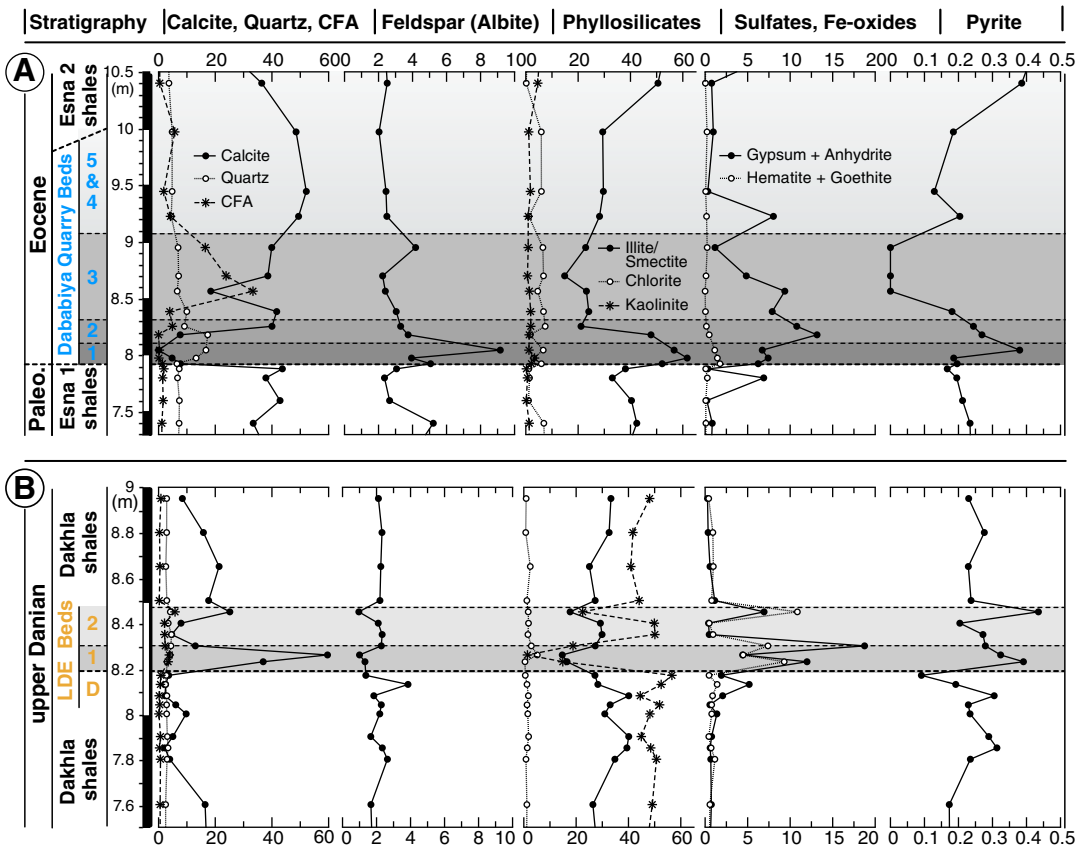

Fig. 5. Abundance of major mineralogical phases of the (A) Q2 PETM and (B) Q3 LDE section based on Rietveld refinement of XRD analysis.

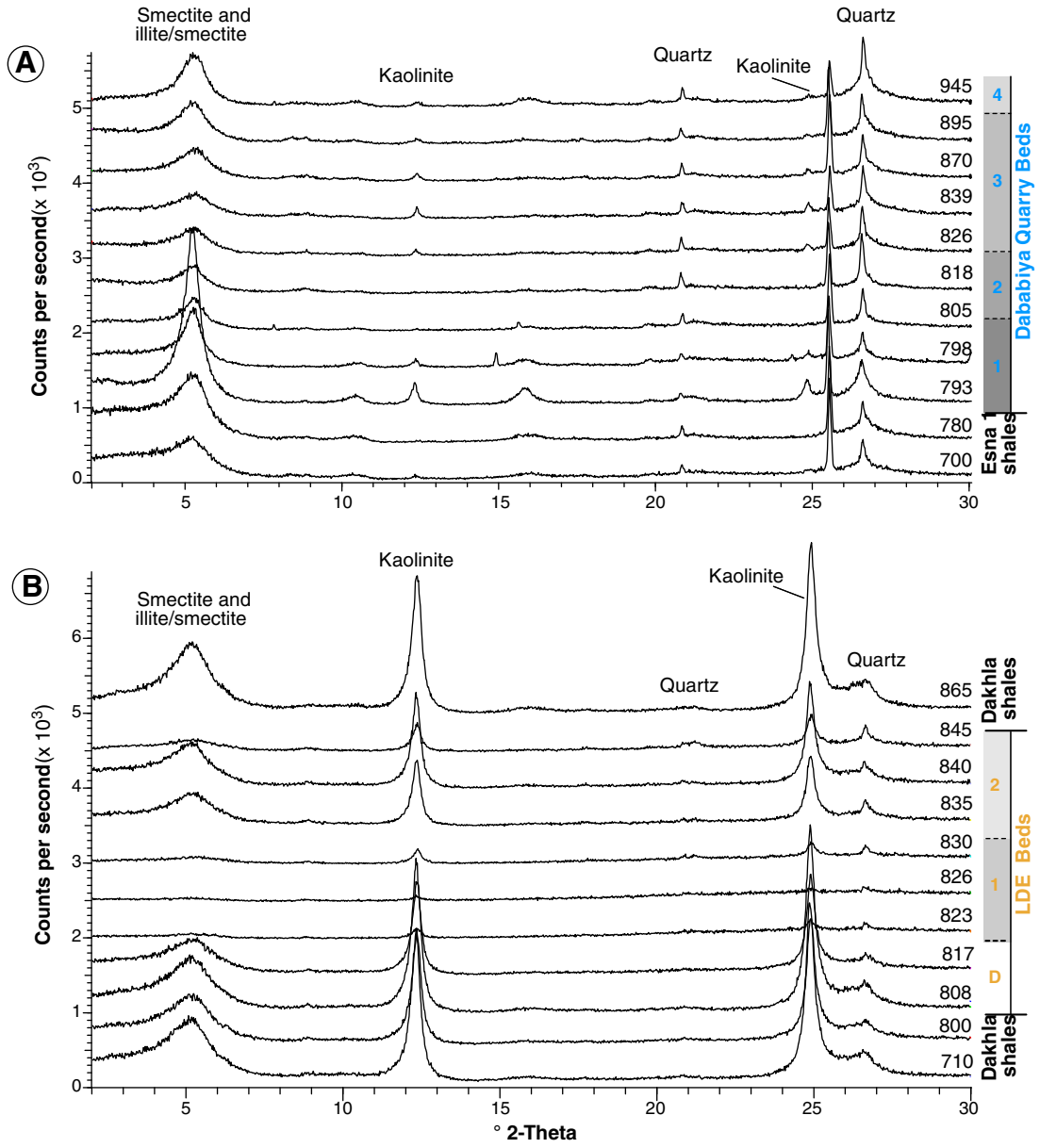

Fig. 6. X-ray diffractometry scans of the decarbonatized, glycolized and oriented <2 μm fraction across the (A) PETM and the (B) LDE in the Qreiya sections.

of kaolinite, which has a lower Si/Al ratio (~1.2) compared to smectite minerals (~2.8) found across the PETM. Across the LDE and PETM event beds, there is a general increase in almost all element/Al ratios except for the decreased K/Al ratio in the LDE bed 1.

The increase of the Si/Al and K/Al ratio within LDE bed 1 may suggest higher quartz and feldspar abundance (Fig. 7, Bengtsson and Stevens, 1998). In contrast, the Ti/Al and Zr/Al, Rb/Al ratios, which are proxies for sediment grain size and heavy mineral content (e.g., Curtis, 1990; Bertrand et al., 1996; Bengtsson and Stevens, 1998), show only very small shifts in the LDE beds (Fig. 7).

The lowered Si/Al ratios may be explained by the disproportional increase of the phyllosilicate vs. the quartz content in PETM bed 1 as also indicated by the mineral abundances (Fig. 7). However, Zr (as well as Ti) tends to be enriched in fine-silty detritus and heavy minerals, whereas Rb and Al are mainly associated with the clay mineral fraction (e.g., Dypvik and Harris, 2001; Rachold and Brumsack, 2001). Thus, the high Zr/Al (and Ti/Al) ratios suggest that also coarse particles were deposited along with the phyllosilicates. In the context of shelf environments, such changes of the detrital input generally reflect increased sedimentation rates (e.g., Murphy et al., 2000), suggesting a pulse-like influx of phyllosilicate-rich, siliciclastic detrital material that is predominantly derived from soils but also from less weathered rocks.

3.4. Redox-sensitive trace elements

For the Qreiya PETM and LDE beds, oxygen-deficiency has been inferred from lithological characteristics (lamination, OM enrichment) and the rare occurrence or absence of benthic foraminifera as outlined in the previous sections. By providing trace element (TE) data, we detail the evolution of redox conditions during these events and address possible causal mechanisms (see Calvert and Pedersen, 1993; Rimmer, 2004; Brumsack, 2006). In Fig. 8, we show TE enrichment factors (EFs) that were calculated in a first step by normalizing each TE to Al, which is assumed to represent the detrital influx. In a second step, these elemental/Al ratios are then compared to typical element/Al ratios of the Dakhla and Esna shales, representing the background sedimentation.

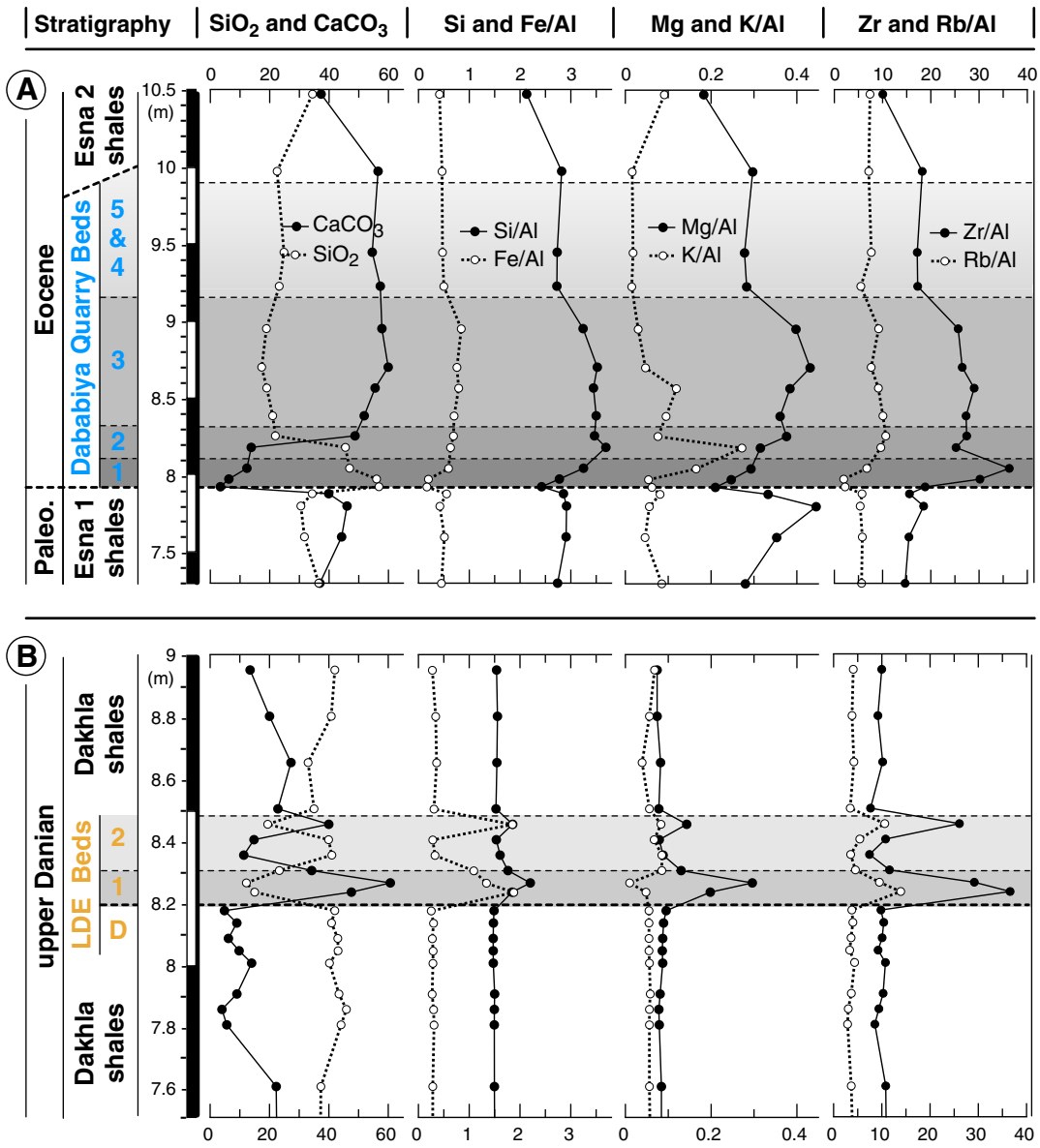

Fig. 7. Selected oxides as well as element/Al ratios and the Zr/Rb ratio to characterize the detrital fraction of the (A) PETM and (B) LDE sediments in the Qreiya sections.

Both, the Q3 LDE beds and the lower part of the Q2 PETM beds show high EFs, though differences in the EFs of individual elements exist between both events. In the Q3 LDE beds, the TE enrichment is mainly confined to two peak phases occurring within bed 1 and in the upper part of bed 2, though gradually increasing TE enrichments occur during the dissolution interval underlying the event bed (Fig. 8). Very high enrichments (>>10-fold) are observed for Zn, V, Ni, Cu, As, U, Cr, while Co, Pb, and Mn show only moderate enrichments. In the Q2 PETM beds the TE enrichment is slightly different: following a gradual increase in bed 1, peak enrichments occur within bed 2 followed by a gradual return to background Esna shale values atop of bed 4 and 5 (Fig. 8). Specifically, V, Zn, and U show a strong (>>10-fold) enrichment, while Cu, Ni, As, and Pb show a moderate enrichment. Notably Cr is strongly enriched in PETM bed 3 while Mn and Co are significantly depleted in bed 1 and 2.

TEs may actually be released and moved during post-depositional oxidation and leaching by pore fluids (Lavergren et al., 2009). However, many TEs are trapped in newly formed iron oxide/phosphate minerals during the oxidative weathering of black shales and thus are fixed within a few centimeters of their original depth of deposition (e.g., Thomson et al., 1998; Tribovillard et al., 2006; Fischer et al., 2009). For the Qreiya LDE and PETM beds, the strong enrichment of redox-sensitive TEs considered being less vulnerable to diagenetic and weathering complications (i.e., U, V, Ni, Cu, Tribovillard et al., 2006) suggests that the general geochemical message is preserved in the sediments, despite a significant weathering influx outlined in the previous section. Consequently, and analogous to observations from other black shales in the geological record, the high EFs of TEs that are redox sensitive and/or sulphide forming (U, V, Cu, Cr, Zn, Ni, Co), and also possible indicators of the organic matter flux to the sediments (Ni and Cu), suggest reducing conditions during deposition (e.g., Brumsack, 2006; Tribovillard et al., 2006; Piper and Calvert, 2009; Jenkyns, 2010). These TEs may either be precipitated as autonomous sulfides (Co, Zn and Pb), coprecipitated with iron sulfides (V, Ni and Cu), and/or were bound to organic matter (U, V, Ni, and Cu). Among the studied trace metals, V and U are reputed as redox-sensitive markers with the least detrital influx (e.g., Algeo et al., 2004; Cruse and Lyons, 2004; Rimmer, 2004; Rimmer et al., 2004; Tribovillard et al., 2006). In the LDE as well as in the PETM beds, V and U are the most enriched elements compared to the background shale values,

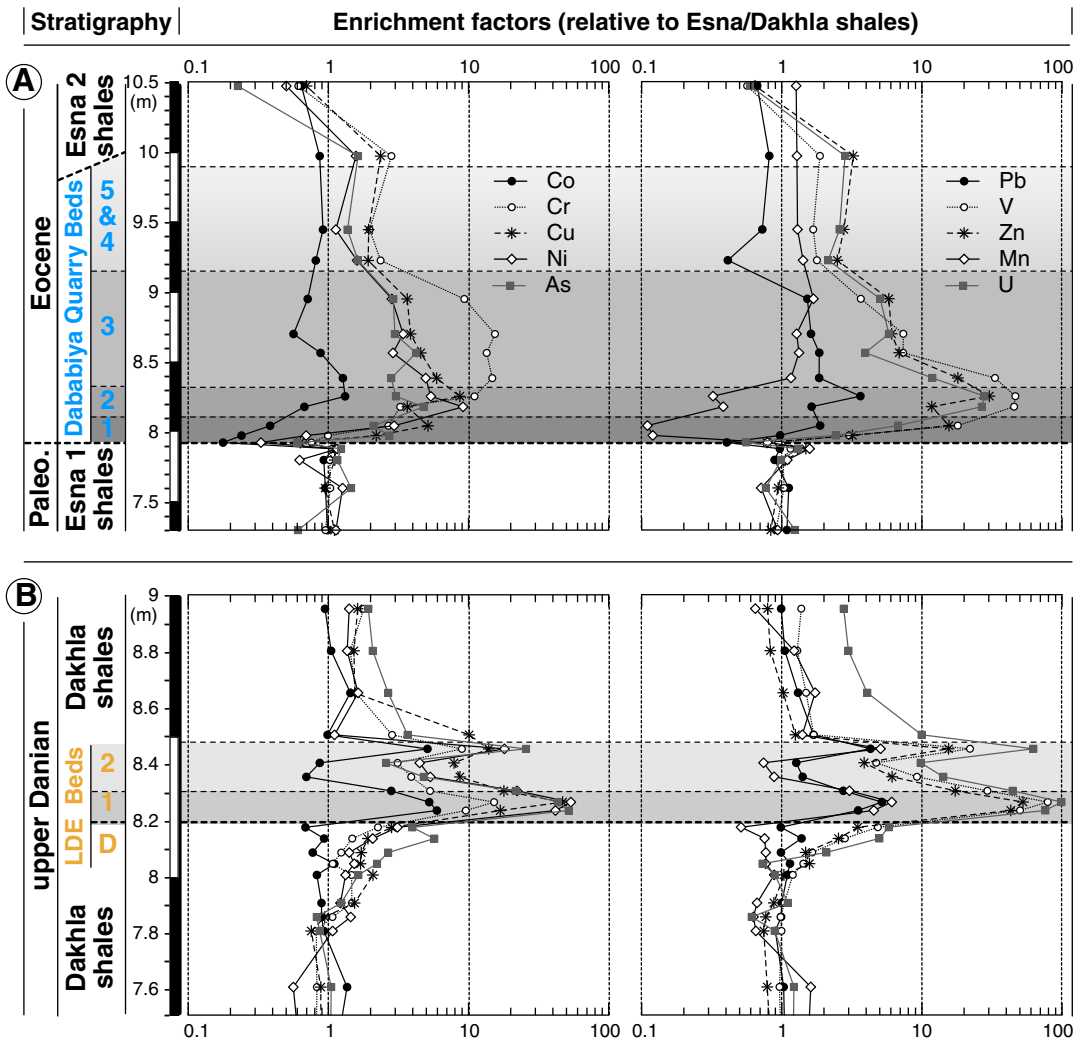

Fig. 8. Enrichment factors of redox-sensitive trace elements for the (A) Q2 PETM and (B) Q3 LDE section.

indicating that the sediments were temporarily depleted in oxygen at the time of deposition (e.g., Brumsack, 2006; Tribovillard et al., 2006). The plots of characteristic geochemical indices, including the Ni/Co, V/Cr, U/Th ratios, and the calculated authigenic U ($U_{auth} = U_{total} - (Th_{total}/3)$) shown in Fig. 9, also supported this interpretation (Jones and Manning, 1994). All of these redox proxies show well-oxygenated conditions for the background sediments of the Dakhla and Esna shales as well as for PETM bed 4 and 5 (Fig. 9). In contrast, high redox indices are observed within bed 1 and on top of bed 2 of the LDE section and within the PETM beds 1 to 3 with peak values during the bed 1 to 2 transition, suggesting generally anoxic conditions during formation of these beds and short ventilation events during bed 3. This interpretation is in agreement with the interpretation of the benthic foraminifera assemblages, since suboxic conditions would have allowed for specialized benthic communities during deposition of PETM bed 1 to 3 and LDE bed 1. The occurrence of a second peak of the redox indices within the top of LDE bed 2 may either reflect a second brief phase of anoxia or reworking and redeposition of LDE bed 1 at the seafloor (see Sprong et al., 2011).

Additional details on the redox conditions may be revealed by considering the enrichment of TEs with strong euxinic affinity (U, V, Zn; Fig. 8) in the LDE beds, compared to the PETM beds, suggesting the possible presence of dissolved sulphide in the water column close to the sediment-water interface during LDE bed 1 (and possibly also at the top of LDE bed 2) (Paillard, 2001; Algeo and Maynard, 2004; Lyons and Severmann, 2006). This interpretation is supported by the concurrent strongly elevated Fe/Al ratios in the LDE beds (Fig. 7). In the absence of data supporting an increase in (iron-rich) detrital material, such extreme high Fe/Al ratios may reflect brief periods of iron scavenged from the euxinic water column during syngenetic pyrite formation and deposition in the underlying sediments (e.g., Lyons and Severmann, 2006). This fits well with nearly all LDE bed 1 planktic foraminifera being filled with ironoxides. Such a Fe augmentation is not only decoupled from the local flux of siliciclastic sediment but also from biogenic inputs (Canfield et al., 1996), and it does appear to be a uniquely euxinic phenomenon (Lyons and Severmann, 2006). Although high degrees of alteration and weathering, as observed in the Qreiya sections, result in mineralogical changes that repartition the elemental constituents, the total amount of iron should remain constant despite any internal redistribution (Lyons and Severmann, 2006).

Finally, the redox conditions may be deduced from the covariance of the Mn and Co in both sections, albeit with contrasting deflections (Mn, Co enrichment during the LDE, depletion within PETM). Mn is frequently depleted in black shales because its oxyhydroxides undergo reductive dissolution and are remobilized as soluble elements (Mn^{2+}, Calvert and Pedersen, 1996; Paillard, 2001). While the Mn depletion of the PETM beds is in good agreement with this mechanism, the relative Mn enrichment in the LDE beds may be explained by the authigenic precipitation of Mn carbonates (e.g., rhodochrosite, Calvert and Pedersen, 1996). Mn is known to co-precipitate under euxinic conditions in the water column with iron and if a considerable mass-flux of

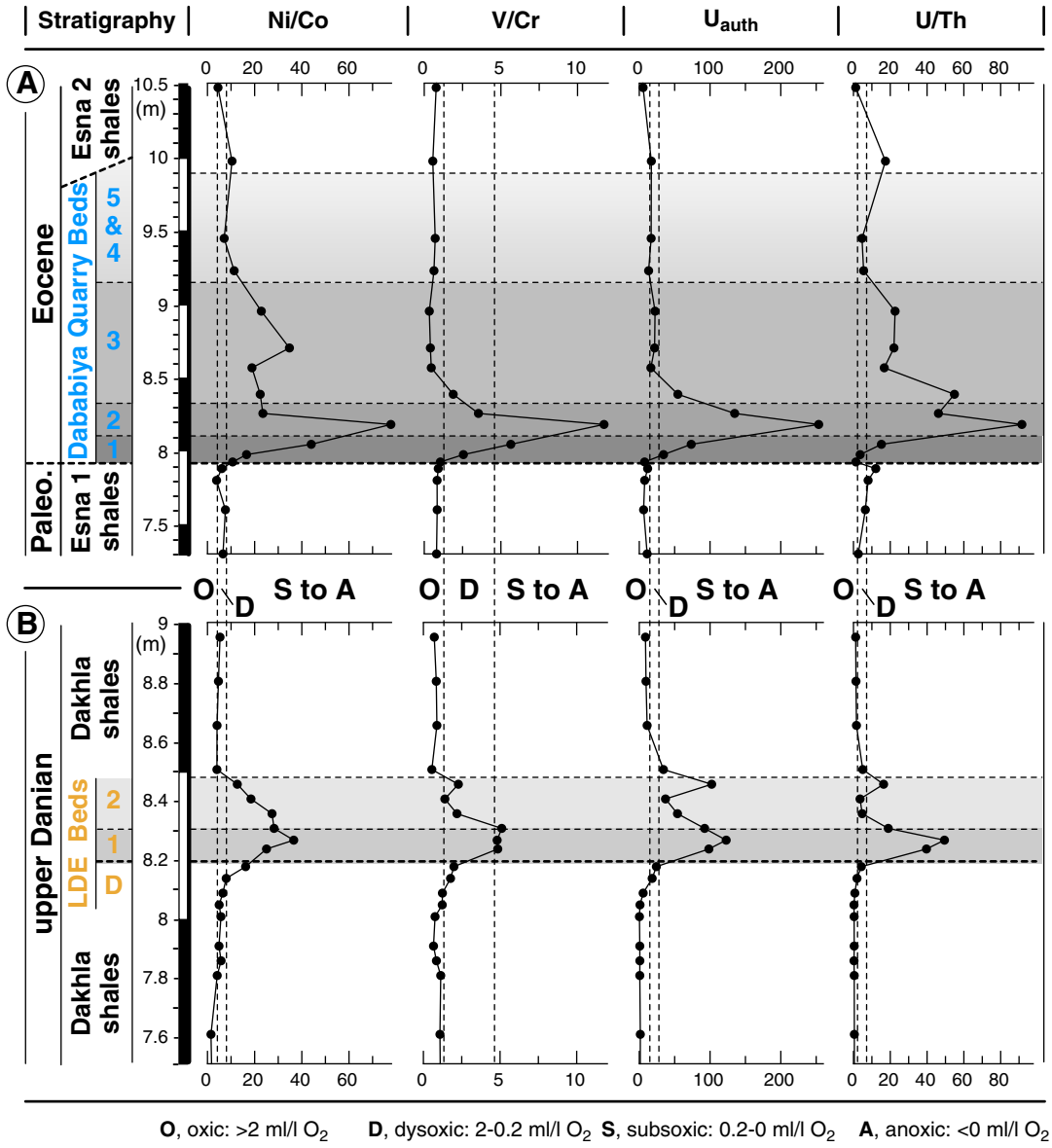

Fig. 9. Compilation of various redox indices (Jones and Manning, 1994) for the (A) Q2 PETM and (B) Q3 LDE section.

Fe-Mn-oxyhydroxides is sustained, a proportion of Mn may be deposited in the sediment even during persistent anoxia (Calvert and Pedersen, 1996).

3.5. Stable isotopes and organic matter

In contrast to the well-known ~3‰ negative carbon isotope excursion of organic carbon at the PETM in Egypt that was confirmed by our study (Fig. 10, see also Dupuis et al., 2003), the isotope chemostratigraphy across the LDE shows a different trend: Our results reveal declining carbon isotope values (from about −25 to −26.7‰) in the interval immediately preceding the LDE beds, followed by an abrupt positive shift to about −23‰ within LDE bed 1. Subsequently, there is a gradual return to pre-marker-bed values of about −26‰, which are reached at about 8.5 m. Further upsection, the $\delta^{13}C_{org}$ values remain in the range around −25‰. These divergent values may suggest that either a different type of organic matter is present at the LDE, compared to the PETM, or that differential organic matter preservation may play a role (Tyson, 1995). However, the petrographic examination of the organic matter in the LDE and PETM events beds shows that identifiable wood or charcoal remains from nearshore or fluvial environments are rare; the bulk of the organic matter is made of finely disseminated black carbon. Upon heating during Rock-Eval analysis (Table 2), samples from the LDE and the PETM beds generally show a low free hydrocarbon release at the S1 peak (around 300 °C) but a maximum amount of hydrocarbons generated through thermal cracking of nonvolatile organic matter at the S2 peak (around 475 °C). Some samples also show a bimodal S2 peak with maxima occurring between 460 °C and 500 °C. The T_{max} values describe the temperature at which the maximum release of hydrocarbons from cracking of kerogen occurs during pyrolysis (top of S2 peak, Tissot and Welte, 1984). Thus, T_{max} is an indication of the stage of maturation of the organic matter and the high values observed in the organic-rich LDE and PETM event beds would correspond to thermal heating of more than 170 °C, which is beyond the oil-window and near the anchimetamorphic zone. Such extreme heating seems highly unrealistic considering the sedimentary overburden in Egypt (less than a few hundred meters, Youssef, 2003). It is also highly unlikely that the Suez Rift System contributed heat to all of these sections. Therefore, we suggest that considerable postsedimentary alteration and oxidation affected the primary deposited organic matter in these

sections, comparable to the weathering effects described above and in agreement with previous Rock-Eval results based on low-resolution sampling of the Qreiya and Nezzi sections (Speijer and Wagner, 2002).

Nevertheless, plotting the oxygen index (OI) and hydrogen index (HI) of the organic-rich samples of the LDE and PETM beds into a modified van Krevelen diagram (Tissot and Welte, 1984) reveals distinct differences between both events bed that are difficult to explain by weathering alone. Fig. 10 shows that the OI and HI values are generally located in the Type III area (Tissot and Welte, 1984), but for the LDE beds the lower HI and higher OI values compared to the PETM beds may suggest a different type of organic matter or a different alteration state (see also Table 2). These differences provide one likely explanation for the divergent changes in organic carbon stable isotope composition observed for the LDE (positive excursion) and PETM (negative anomaly) beds (Fig. 10) as well as for the contrasting correlation of the carbon isotope values with the organic matter content (Table 2, Fig. 10).

4. Discussion

4.1. Sea-level changes

Analogous to other PETM sites in Egypt (Speijer and Wagner, 2002; Ernst et al., 2006), the benthic faunal assemblages indicate a scenario of sea-level fall (interpreted as late highstand systems tract, "HST") before deposition of the Q2 PETM beds during a rapidly rising sea level (transgressive systems tract; "TST"). This transgression is associated with a brief phase with absence of benthic life, followed by incursion of opportunistic benthic species from shallower parts of the shelf and return to background sedimentation conditions (Fig. 4). This sequence stratigraphic setting suggests that the base of the PETM corresponds to a sequence boundary (Speijer and Wagner, 2002), although the absence of benthic life hampers a detailed paleo-waterdepth reconstruction across the lower part of the PETM. For the Q3 LDE beds, the general pattern of benthic assemblage changes is very similar, suggesting an analogous pattern anoxia concomitant to sea-level changes (Fig. 4, Speijer, 2003; Sprong et al., 2011).

4.2. Changes in clastic influx

One characteristic feature of the PETM record at Gebel Qreiya sites that has not been observed at the LDE is a strong detritus pulse concurrent to the onset the transient warming event. A remarkably similar detritus pulse is reflected in the mineralogical and geochemical data from the Dababiya PETM section which is situated about 120 km to the southwest in slightly shallower marine settings (Dupuis et al., 2003; Ernst et al., 2006; Schulte et al., 2011). In addition, corresponding

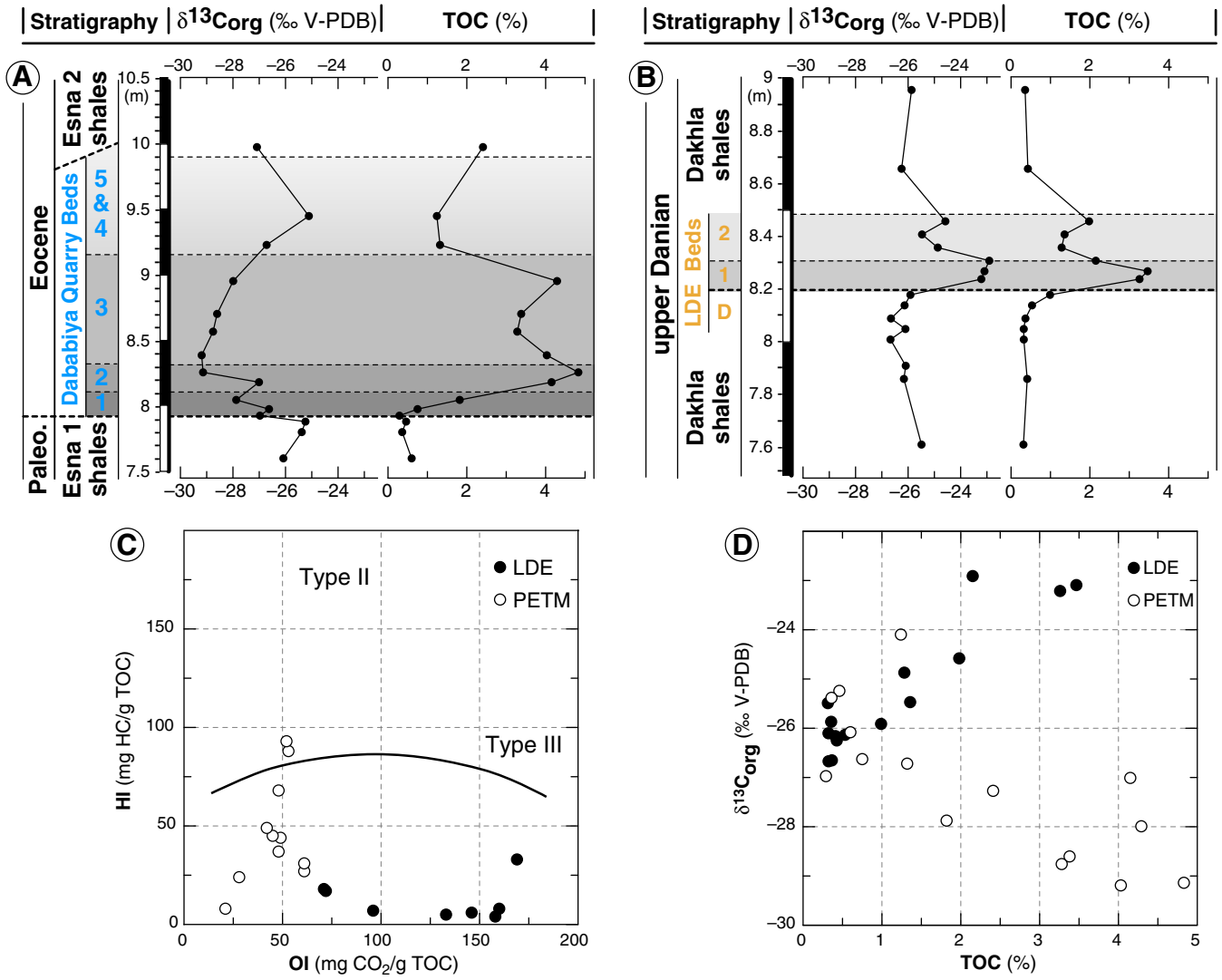

Fig. 10. Results from the stable carbon isotope analysis of organic matter and for (A) the Q2 PETM and (B) the Q3 LDE section. (C) Modified Van-Krevelen Diagram showing the OI and HI values for samples from the LDE and PETM event bed and (D) crossplot of the $\delta^{13}C_{org}$ values against the TOC.

Table 2
Results from the carbon isotopes of organic matter and Rock-Eval analysis.

Sample	Bed	δ^{13}Corg	S1	S2	S3	T_{max}	TOC	OI	HI
		‰V-PDB	(mg/g)	(mg/g)	(mg/g)	(°C)	(%)	($mgCO_2$/g TOC)	(mgHC/g TOC)
Q3 DS 51		-26.03	0.06	0.01	3.7	307	0.36	1039	3
Q3 DS 47		-26.25	0.06	0	3.47	x	0.43	813	0
Q3 DS 45		-24.58	0.08	0.07	3.12	355	1.98	158	4
Q3 DS 44		-25.47	0.07	0.08	1.98	372	1.36	146	6
Q3 DS 43	2	-24.87	0.06	0.06	1.71	418	1.28	133	5
Q3 DS 42	2	-22.91	0.1	0.15	2.07	467	2.15	96	7
Q3 DS 41	1	-23.09	0.11	0.6	2.5	452	3.47	72	17
Q3 DS 40	1	-23.21	0.12	0.58	2.33	443	3.26	71	18
Q3 DS 39		-25.91	0.13	0.33	1.67	329	0.99	169	33
Q3 DS 38		-26.13	0.06	0.04	0.85	375	0.53	160	8
Q3 DS 37		-26.65	0.07	0	1.18	x	0.37	323	0
Q3 DS 36		-26.1	0.07	0	0.89	x	0.32	276	0
Q3 DS 35		-26.67	0.05	0	1.45	x	0.32	449	0
Q3 DS 33		-26.16	0.07	0	0.92	x	0.41	224	0
Q3 DS 31		-25.49	0.08	0	1.29	x	0.31	411	0
Q2 PE 31	4 & 5	-27.34	0.09	1.06	1.17	451	2.41	49	44
Q2 PE 30	4 & 5	-24.11	0.06	0.34	0.76	459	1.24	61	27
Q2 PE 29	4 & 5	-27.51	0.06	0.41	0.8	459	1.32	61	31
Q2 PE 28	4 & 5	-27.99	0.11	1.05	1.21	453	4.29	28	24
Q2 PE 27	3	-28.6	0.11	1.51	1.51	472	3.38	45	45
Q2 PE 26	3	-28.76	0.09	1.6	1.37	456	3.28	42	49
Q2 PE 25	3	-29.19	0.1	3.53	2.14	445	4.03	53	88
Q2 PE 24	3	-29.14	0.11	4.51	2.5	441	4.83	52	93
Q2 PE 23	2	-27.01	0.11	2.84	2.01	487	4.15	48	68
Q2 PE 22	2	-27.88	0.07	0.67	0.87	470	1.82	48	37
Q2 PE 21	1	-26.63	0.05	0.06	0.16	376	0.75	21	8
Q2 PE 20	1	-26.97	0.05	0	0.09	x	0.29	31	0
Q2 PE 19		-25.24	0.06	0.06	0.36	363	0.46	79	13
Q2 PE 18		-25.38	0.04	0	0	x	0.36	0	0
Q2 PE 17		-26.08	0.06	0.13	0.89	398	0.6	148	22

Rock-Eval below detection limit since TOC below 0.5%.
T_{max} probably not correct since intensity to low.
T_{max} not determinable since no S2-value exists.

observations have been reported from several other PETM shelf environments globally (e.g., Cramer et al., 1999; Schmitz et al., 2001; Crouch et al., 2003). The increased terrigeneous fluxes may have also diluted marine carbonate contents in shelf environments providing one explanation for the extremely low carbonate contents of these sediments (e.g., Dickens, 2001). The strong increase in siliciclastic flux may be either explained by a rapid sea-level lowering or a strongly enhanced terrestrial discharge resulting from a strongly accelerated hydrological cycle and intensified chemical weathering in the subtropics induced by global warming (e.g., Schmitz et al., 2001), which has been shown by Os isotopes (Ravizza et al., 2001). We consider the former scenario rather unlikely since regional and global records suggest a eustatic rise during the PETM, beginning several thousand years before the globally recorded CIE (Speijer and Morsi, 2002; Speijer and Wagner, 2002; Sluijs et al., 2008). Since transgressive settings are usually associated with sediment starvation on the shelf (e.g., Cattaneo and Steel, 2003),

a sea-level rise concomitant to high detrital flux as observed at the Qreiya section would require a dramatically increased terrestrial discharge during the onset of the PETM. The subsequent gradual decrease of the Ti/Al ratio within beds 2 and 3 suggests gradually decreasing detrital input before reaching background Esna shale values in beds 4 and 5 (Fig. 7). This decreasing siliciclastic flux due to lowered terrestrial discharge and/or sea-level rise may be one explanation for the simultaneous appearance of carbonate, OM, and phosphates as significant sedimentary constituents within beds 2 and 3. In addition, dilution by an increasing biogenic flux may also account for these changes though the decreasing Ti/Al ratios during this interval suggest that this factor was not exclusively responsible for clastic dilution.

The absence of a distinct pulse of siliciclastic material during deposition of the LDE bed may be the consequence of a less severe environmental impact of this hyperthermal event compared to the PETM. Such an interpretation is in line with a recently published first stable isotope dataset from the Central Pacific that indicates a transient warming of bottom waters by only 2 °C during the LDE (Fig. 2, Westerhold et al., 2011), by contrast for the PETM warming of bottom waters by 5 to 8 °C has been proposed (Sluijs et al., 2007). Therefore, it is likely that the environmental changes during the LDE are of significantly lower magnitude than those observed during the PETM.

4.3. Anoxia and black shale formation

For the PETM the proxy record suggests a brief euxinic phase superimposed on a longer interval with anoxic conditions, very similar to the Dababiya PETM section (Ernst et al., 2006; Schulte et al., 2011). Further evidence for shelf anoxia (and even euxinic conditions) comes from black shales in sections from the eastern Tethys (Bolle et al., 2000; Gavrilov et al., 2003) and the semi-enclosed shelf areas of the Arctic Ocean (Sluijs et al., 2006). Moreover, the presence of irregular highly diverse magnetite-forming organisms from the New Jersey shelf (Schumann et al., 2008; Kopp et al., 2009) suggests development of a thick suboxic zone during the onset of the PETM, albeit not associated with a strong OM enrichment. In addition, oxygen deficiency (but no anoxia) in deep and intermediate waters appears to have been widespread at the PETM (Bralower et al., 1997; Katz et al., 1999; Thomas, 2007; Chun et al., 2010; Nicolo et al., 2010) and may have resulted from a combination of ocean warming and CH_4 oxidation (e.g., Dickens et al., 1995).

For the LDE, our multi-proxy record provides evidence for two brief periods of anoxic (also possibly euxinic) conditions and enhanced organic matter flux. Both anoxic periods were separated by a period (lower part of LDE bed 2) when oxygenation at the seafloor improved, at least temporarily, allowing development of benthic life (gastropods, bivalves, benthic foraminifera, Fig. 4). In contrast to the PETM, low oxygen conditions have so far not been described from deep-sea sites spanning the LDE (Westerhold et al., 2011). This absence may again attest to the smaller environmental impact of the LDE compared to the PETM. However, an important additional detail of both, the LDE and the PETM event bed in the Qreiya sections is that reducing conditions developed gradually in the interval prior to deposition of the organic rich beds. Consequently, the organic-enrichment may be a consequence and not the cause of the development of anoxia.

4.4. Origin of organic matter and the stable isotope signature

As outlined before, the negative $\delta^{13}C_{org}$ anomaly observed at the Q2 PETM beds is very similar to that observed other PETM sections in the Qreiya area (Knox et al., 2003) or at Dababiya (Dupuis et al., 2003). However, it is remarkable, that there is a negative correlation of the TOC content with the $\delta^{13}C_{org}$ signal (Figs. 4 and 10). The Rock-Eval data show that the OM represents altered kerogen, though the higher hydrogen index values suggest that it is significantly less degraded than at the LDE (Table 2). The high OI and low HI values of the PETM samples may suggest that the original kerogen derived mostly from higher (terrestrial) plant biomass which has a lower hydrogen content compared to marine bacteria and phytoplankton. Nevertheless, a contribution from marine OM is also possible and may be one explanation for the peak negative $\delta^{13}C_{org}$ values within PETM bed 2 concurrent to the strong increase in TOC, since marine OM generally has significantly lower $\delta^{13}C_{org}$ values as shown above (Fig. 10).

For the Dababiya PETM section, palynofacies analysis revealed that most of the organic matter consists of black brown highly oxidized woody tissue fragments and some coal-particles (Dupuis et al., 2003). However, only three samples were investigated across the PETM beds in the Dababiya section: One sample from the very base of bed 1 (terrestrial OM), one sample from the middle part of bed 3 with 22% algae material (yellow amorphous organic matter), and one sample from bed 4 (terrestrial OM). Therefore, no palynofacies data exists for the critical interval encompassing beds 1 to 3, and it remains unclear to which degree changes in the terrestrial vs. marine organic matter contributed to the onset and peak of the carbon isotope excursion in this section and consequently, to which degree this carbon isotope excursion reflects the CIE; a question that would also apply to the carbon isotope chemostratigraphy of the Q2 PETM section. The shape and magnitude of the excursion is remarkably similar to the globally observed CIE (see Magioncalda et al., 2004), so that Dupuis et al. (2003) proposed that the PETM isotope anomaly observed at the Dababiya section reflects the globally observed CIE. We concur with this interpretation, but we suggest supplementary investigations on the OM to determine changes in type, abundance, and preservation across the Q2 PETM section.

For the LDE, recent studies have revealed an about 1–2‰ negative carbon isotope excursion recorded in benthic foraminifera shells (Fig. 4, Bornemann et al., 2009; Westerhold et al., 2011). However, our results revealed that the LDE beds in the Qreiya area show a pronounced 3‰ positive $\delta^{13}C_{org}$ anomaly in the Q3 LDE beds. This large positive excursion is in strong contrast to the low magnitude negative carbon isotope excursion observed in carbonates and also in contrast to the observations at the PETM where both, organic and inorganic carbon isotope values show a negative excursion. Therefore, we suggest that local factors may play a dominant role. One explanation for the positive $\delta^{13}C_{org}$ anomaly in the Q3 LDE beds may be a dominance of terrigeneous plant material since pre-Neogene organic matter of phytoplanktic and bacterial origin usually shows significantly lighter values of −25 to −32‰ $\delta^{13}C_{org}$ compared to heavier C3 plant-derived organic matter (−20 to −26‰, Tyson, 1995). This interpretation is in agreement with abundant small plant fragments that have been observed within the LDE bed 1 in other outcrops from the Qreiya area (M.-P. Aubry pers. commun.). This increase in the amount of terrestrial OM may have resulted from a change of the sediment provenance (e.g., more wind-blown terrestrial OM), a decrease in sedimentation rate (condensation), a less efficient decomposition of terrestrially derived organics under low-oxygen conditions (Hedges et al., 1988; Canfield, 1994), or a combination of these factors. This scenario is supported by our detrital proxy analysis, showing not only strongly decreased sedimentation rates (starvation) but also development of anoxic conditions at the onset of the LDE.

Alternatively, a shoaling chemocline in a thermally stratified epeiric shelf sea may explain the increase in the $\delta^{13}C_{org}$ values. A shallow chemocline is more vulnerable to episodically occurring turbulent mixing, releasing sufficient nutrients to sustain higher primary productivity, resulting in relatively higher $\delta^{13}C_{org}$ values (Küspert, 1982; Sælen et al., 2000). Although shallowing of the chemocline is difficult to assess with the current dataset, micropaleontological proxies suggest stable stratification of the southern Tethyan shelf, which increased productivity of surface waters during the LDE (Guasti, 2005).

An unequivocal differentiation between these scenarios for the Q3 LDE beds is, however, difficult and the possible factors including either

increased terrestrial OM, water mass stratification, and/or increased surface productivity (or a combination thereof) must be determined by subsequent analysis of organic matter (preferably on a molecular/biomarker level).

4.5. Phosphate recycling and sequestration

The sedimentary record of several episodes of anoxia in the geological record suggest that P cycling and regeneration can affect primary productivity and carbon cycling on regional to global scales (Algeo and Ingall, 2007; Kraal et al., 2010). A useful proxy for redox-dependent P recycling and sequestration is the C_{org}/P ratio based on the assumption that detrital P is low (e.g., Algeo and Ingall, 2007; Kraal et al., 2010). The PETM beds show a relatively complex P recycling and burial history. Microscopic investigations (Knox et al., 2003; Soliman, 2003) as well as our own analysis of the phosphatic fraction from the Q2 PETM section showed that the beds 1 and 2 include only sparse, randomly distributed mm-sized P-nodules and fish debris in agreement with low P concentrations (Figs. 4 and 7). Gradually increasing C_{org}/P ratios during the onset of the PETM therefore may reflect decreased sedimentary P retention capacity. Thus feedbacks between decreasing bottom water oxygenation recorded in these beds and P recycling from the sediment could have increased the dissolved oceanic P reservoir. This may have promoted productivity of southern Tethyan surface waters during the peak interval of fully anoxic (euxinic) conditions (bed 2), provided the nutrient P is upwelled into the photic zone (e.g., Van Cappellen and Ingall, 1994; Sageman et al., 2003). The subsequent PETM recovery phase shows a significant increase in P concentrations (see Figs. 4 and 7) concurrent to a shift from fully anoxic to (at least periodically) dysoxic to anoxic conditions, when $\delta^{13}C_{org}$ values start to increase, TE enrichments decreased, and benthic life improved. Thus, the low C_{org}/P ratios in this interval show a shift from P recycling to P sequestration (Fig. 9) since less P is commonly released from sediments under oxygenated waters.

This scenario for increased P and OM burial may have been forced by upwelling of nutrient-rich deep water, similar to sediments developing beneath upwelling zones (e.g., Brumsack, 2006). However, the Qreiya PETM site may have been too remote from the deep ocean to support a classical upwelling setting (see discussion in Schulte et al., 2011). Therefore, we suggest that nutrients sustaining the productivity in the surface water were delivered from coastal regions. A similar interpretation has been put forward for the regionally extensive PETM black shales on the northeastern Tethyan shelf by Gavrilov et al. (2003).

In contrast to the P chemostratigraphy across the Q2 PETM section, the Q3 LDE section shows only a distinct, yet small P enrichment that is confined to the interval immediately below (some fish remains) and within (fish remains and few P-nodules) the LDE bed 1 (Figs. 5 and 7). Although enhanced preservation of fish debris may become an important reactive P sink in sediments during periods of anoxia (Slomp and Van Cappellen, 2007), the amount of P burial recorded in the Q3 LDE beds is certainly not relevant for the local P cycle or for P upwelling in the photic zone during upwelling.

5. Depositional scenario

A synoptic view of the multiproxy data provided for the LDE and PETM beds suggests that rapidly rising sea-level was probably an important factor controlling burial of organic matter during both events in parts of the Tethyan realm. The development of anoxic conditions during transgressions has been observed frequently in the geological record (e.g., Wignall and Maynard, 1993). Although the absolute amplitude of sea-level rise during the PETM is only about 20 to 30 m (Speijer and Morsi, 2002; Sluijs et al., 2008), such a rise would result in a considerable transgression (shoreline shift) on the very gently inclined epicontinental Egyptian shelf. According to the scenario outlined by Erbacher et al. (1996) and Sageman et al. (2003), a sea-level rise leads to sediment starvation and increased organic carbon concentration in surface sediments due to less dilution. Even more important, seasonal (or longer term) mixing of the water column decreases since a larger body of water becomes isolated from surface waters, allowing a longer build-up interval for remineralizing nutrients. In this scenario, episodic mixing of P-rich bottom-waters or nutrients delivered by fluvial discharge promote productivity. Ultimately, increased sediment delivery during the highstand systems tract, in concert with improved water column mixing, resulted in restored oxygen supply that overtakes demand and terminated the enhanced carbon burial.

In addition to sea-level rise, the massive warming during the PETM promotes fresh-water and nutrient discharge, which, in turn, effectively increases water column stratification and primary productivity. Analogous to recent regional (Rabalais et al., 2002) and global (e.g., Rabalais et al., 2009) scenarios developed for the ongoing global warming, shelf systems are very sensitive to changes of these variables. The negative consequences of increased nutrient supply and stratification may be temporarily compensated by stronger or more frequent tropical storm activity in low and mid-latitudes (Rabalais et al., 2009). Specifically, on the rather restricted southern Tethyan shelf, this mechanism may have been quite effective.

Therefore, a range of factors may have acted together and pushed the southern Tethyan shelf to oxygen-deprivation during both events. By integrating these considerations, we provide a depositional scenario for the OM-rich LDE beds and refine existing depositional models (Speijer and Wagner, 2002) for the black shales at the PETM as follows:

(1) During the pre-PETM and pre-LDE interval, bioturbation and absence of TE enrichment show that there was sufficient, albeit low sea-floor oxygenation as indicated by benthic foraminifera assemblages. The cosmopolitan microfauna suggests a good connection to the open Tethyan Ocean, despite the presence of extensive swells and carbonate platforms to the north and northwest along the unstable shelf (Salem, 1976).
(2) At the onset of the PETM, a major pulse of detrital input started that was not observed at the LDE. However, lamination and absence of benthic fauna recorded in both, the PETM as well as the LDE event beds, suggest the development of anoxic conditions as also supported by the enrichment in TEs and OM. Advection of OMZ waters onto the shelf may have promoted the oxygen-deficiency, while the extreme terrestrial discharge may have inhibited productivity and/or diluted organic carbon burial. During both events, a rapid sea-level rise led to sediment starvation and possibly enhanced water column stratification, promoting the development of anoxic (or even euxinic) conditions.
(3) The onset of the decline in $\delta^{13}C_{org}$ values (recovery phase) at the LDE is marked by a rapid return to better-oxygenated conditions without any significant enrichment in TEs and OM. In contrast, the PETM features a prolonged interval associated with slightly improved (probably seasonally enhanced) sea floor oxygenation, albeit oxygen deprived conditions still dominate. Thus, sediment starvation and inflow of nutrient-rich water persisted and led to accumulation of carbonate-, phosphate-, and OM-rich sediments (bed 3). While the LDE features a second brief interval of OM and TE enrichment and elevated carbon isotope values, the late recovery phase of the PETM is characterized by further improvement of oxygenation and gradual restoration of pre-PETM settings (beds 4 and 5).

Considering the implications of our scenario for the global carbon budget during these hyperthermals, the areal extend of the Egyptian shelf is certainly not large enough to have a significant impetus on global carbon cycling. However, a model describing the carbon burial during sea level rise was introduced by Bjerrum et al. (2006). These authors proposed that the increase in organic carbon burial resulting

from a 20 to 30 m sea level rise lasting less than 200 ky is equivalent to a carbon isotope event of +0.5 to +1‰. Moreover, by considering evidence for excess burial of organic matter in numerous PETM sections from the northeastern Tethys (Caucasus, Turkmenia, Precaspian, Tadzhik depression (Bolle et al., 2000; Gavrilov et al., 2003), the New Jersey shelf (John et al., 2008), and the Arctic Ocean (Sluijs et al., 2006), this mechanism would "kick-in" immediately when global warming has forced a sea-level rise and nutrient supply by enhanced terrestrial discharge increased. Consequently, such excess carbon burial may have asserted a significant feedback effect terminating the PETM, and possibly also the LDE as suggested herein.

6. Conclusions

We conclude that the PETM as well as the LDE are both associated with a rapid sea-level rise during their onset. Both events show the development of a brief phase of anoxic and mostly likely even euxinic conditions concurrent to sea-level rise and warming. Moreover, the PETM record at Gebel Qreiya shows many characteristics of a hyperthermal event that are also recognized in other shelf sections globally. The LDE record is very similar in several aspects, providing further support for a transient warming event, albeit of smaller magnitude. We emphasize, however, that the sedimentary record of both events shares many characteristics with thin transgressive black shales observed in the geological record. Therefore, sea-level change was probably the master variable controlling enhanced carbon burial on the southwestern Tethyan shelf. In concert with similar observations from a really extensive black shales in other Tethyan regions, we suggest that this mechanism may be one important factor for the removal of excess carbon during the early Paleogene hyperthermal events.

Acknowledgments

P.S. thanks the Herta and Hartmut Schmauser Stiftung from the University of Erlangen for the support. We acknowledge Mohammed Youssef (University Qena, Egypt) for providing support during fieldwork and Michael Joachimski (University Erlangen, Germany) for the discussion on the stable isotope analysis. We are also grateful to the reviewers and to the editor Dave Bottjer for the constructive comments.

References

Agnini, C., Macrì, P., Backman, J., Brinkhuis, H., Fornaciari, E., Giusberti, L., Luciani, V., Rio, D., Sluijs, A., Speranza, F., 2009. An early Eocene carbon cycle perturbation at ~52.5 Ma in the Southern Alps: chronology and biotic response. Paleoceanography 24, PA2209. http://dx.doi.org/10.1029/2008PA001649.

Algeo, T.J., Ingall, E.D., 2007. Sedimentary C_{org}:P ratios, paleocean ventilation, and Phanerozoic atmospheric pO_2. Palaeogeogr. Palaeoclimatol. Palaeoecol. 256 (3–4), 130–155. http://dx.doi.org/10.1016/j.palaeo.2007.02.029.

Algeo, T.J., Maynard, J.B., 2004. Trace-element behavior and redox facies in core shales of Upper Pennsylvanian Kansas-type cyclothems. Chem. Geol. 206 (3–4), 289–318. http://dx.doi.org/10.1016/j.chemgeo.2003.12.009.

Algeo, T.J., Schwark, L., Hower, J.C., 2004. High-resolution geochemistry and sequence stratigraphy of the Hushpuckney Shale (Swope Formation, eastern Kansas): implications for climato-environmental dynamics of the Late Pennsylvanian Midcontinent Seaway. Chem. Geol. 206 (3–4), 259–288. http://dx.doi.org/10.1016/j.chemgeo.2003.12.028.

Arenillas, I., Molina, E., Ortiz, S., Schmitz, B., 2008. Foraminiferal and $\delta^{13}C$ isotopic event-stratigraphy across the Danian–Selandian transition at Zumaya (northern Spain): chronostratigraphic implications. Terra Nova 20 (1), 38–44. http://dx.doi.org/10.1111/j.1365-3121.2007.00784.x.

Aubry, M.-P., Ouda, K., Dupuis, C., Berggren, W.A., Van Couvering, J.A., 2007. The Global Standard Stratotype Section and Point (GSSP) for the base of the Eocene Series in the Dababiya section (Egypt). Episodes 30 (4), 271–286.

Bains, S., Norris, R.D., Corfield, R.M., Faul, K.L., 2000. Termination of global warmth at the Paleocene/Eocene boundary through productivity feedback. Nature 407, 171–174. http://dx.doi.org/10.1038/35025035.

Bengtsson, H., Stevens, R.L., 1998. Source and grain-size influences upon the clay mineral distribution in the Skagerrak and northern Kattegat. Clay Minerals 33 (1), 3–13. http://dx.doi.org/10.1180/000985598545381.

Berggren, W.A., Pearson, P.N., 2005. A revised tropical to subtropical Paleogene planktonic foraminiferal zonation. J. Foraminifer. Res. 35 (4), 279–298. http://dx.doi.org/10.2113/35.4.279.

Bergmann, J., Friedel, P., Kleeberg, R., 1998. BGMN — a new fundamental parameter based Rietveld program for laboratory X-ray sources, its use in quantitative analysis and structure investigations. Commission of Powder Diffraction. International Union of Crystallography, CPD Newsletter, 20, pp. 5–8.

Bernaola, G., Baceta, J.I., Orue-Etxebarria, X., Alegret, L., Martín-Rubio, M., Arostegui, J., Dinarès-Turell, J., 2007. Evidence of an abrupt environmental disruption during the mid-Paleocene biotic event (Zumaia section, western Pyrenees). Geol. Soc. Am. Bull. 119 (7), 785–795. http://dx.doi.org/10.1130/B26132.1.

Bertrand, P., Shimmield, G., Martinez, P., Grousset, F., Jorissen, F., Paterne, M., Pujol, C., Bouloubassi, I., Menard, P.B., Peypouquet, J.-P., Beaufort, L., Sicre, M.-A., Lallier-Verges, E., Foster, J.M., Ternois, Y., 1996. The glacial ocean productivity hypothesis: the importance of regional temporal and spatial studies. Mar. Geol. 130 (1–2), 1–9. http://dx.doi.org/10.1016/0025-3227(95), 00166-2.

Bjerrum, C.J., Bendtsen, J., Legarth, J.J.F., 2006. Modeling organic carbon burial during sea level rise with reference to the Cretaceous. Geochem. Geophys. Geosyst. 7, Q05008. http://dx.doi.org/10.1029/2005GC001032.

Bolle, M.P., Pardo, A., Hinrichs, K.U., Adatte, T., von Salis, K., Burns, S.J., Keller, G., Muzylev, N., 2000. The Paleocene–Eocene transition in the marginal northeastern Tethys (Kazakhstan and Usbekistan). Int. J. Earth Sci. 89 (2), 390–414. http://dx.doi.org/10.1007/s005310000092.

Bornemann, A., Schulte, P., Sprong, J., Steurbaut, E., Youssef, M., Speijer, R.P., 2009. Latest Danian carbon isotope anomaly and associated environmental change in the southern Tethys (Nile Basin, Egypt). J. Geol. Soc. Lond. 166 (6), 1135–1142. http://dx.doi.org/10.1144/0016-76492008-104.

Bralower, T.J., Thomas, D.J., Zachos, J.C., Hirschmann, M.M., Röhl, U., Sigurdsson, H., Thomas, E., Whitney, D.L., 1997. High-resolution records of the late Paleocene thermal maximum and circum-Caribbean volcanism: is there a causal link? Geology 25 (11), 963–966. http://dx.doi.org/10.1130/0091-7613(1997)025<0963:HRROTL>2.3.CO;2.

Bralower, T.J., Premoli-Silva, I., Malone, M.J., Scientific Participants of ODP Leg 198, 2002. New evidence for abrupt climate change in the Cretaceous and Paleogene: an ocean drilling program expedition to Shatsky Rise, northwest Pacific. GSA Today 12 (4), 4–10. http://dx.doi.org/10.1130/1052-5173(2002)012<0004:NEFACC>2.0.CO;2.

Brumsack, H.J., 2006. The trace metal content of recent organic carbon-rich sediments: implications for Cretaceous black shale formation. Palaeogeogr. Palaeoclimatol. Palaeoecol. 232 (2–4), 344–361. http://dx.doi.org/10.1016/j.palaeo.2005.05.011.

Calvert, S.E., Pedersen, T.F., 1993. Geochemistry of recent oxic and anoxic marine sediments: implications for the geological record. Mar. Geol. 113 (1–2), 67–88. http://dx.doi.org/10.1016/0025-3227(93)90150-T.

Calvert, S.E., Pedersen, T.F., 1996. Sedimentary geochemistry of manganese: implications for the environment of formation of manganiferous black shales. Econ. Geol. 91 (1), 36–47. http://dx.doi.org/10.2113/gsecongeo.91.1.36.

Canfield, D.E., 1994. Factors influencing organic carbon preservation in marine sediments. Chem. Geol. 114 (3–4), 315–329. http://dx.doi.org/10.1016/0009-2541(94), 90061-2.

Canfield, D.E., Lyons, T.W., Raiswell, R., 1996. A model for iron deposition to euxinic Black Sea sediments. Am. J. Sci. 296 (7), 818–834. http://dx.doi.org/10.2475/ajs.296.7.818.

Cattaneo, A., Steel, R.J., 2003. Transgressive deposits: a review of their variability. Earth Sci. Rev. 62 (3–4), 187–228. http://dx.doi.org/10.1016/S0012-8252(02), 00134-4.

Cheburkin, A.K., Shotyk, W., 1996. An energy-dispersive miniprobe multielement analyzer (EMMA) for direct analysis of Pb and other trace elements in peats. Fresenius J. Anal. Chem. 354 (5), 688–691. http://dx.doi.org/10.1007/s0021663540688.

Chun, C.O.J., Delaney, M.L., Zachos, J.C., 2010. Paleo-redox changes across the Paleocene–Eocene Thermal Maximum, Walvis Ridge (ODP Sites 1262, 1263, and 1266): evidence from Mn and U enrichment factors. Paleoceanography 25 (4), PA4202. http://dx.doi.org/10.1029/2009PA001861.

Coccioni, R., Frontalini, F., Bancalà, G., Fornaciari, E., Jovane, L., Sprovieri, M., 2010. The Dan-C2 hyperthermal event at Gubbio (Italy): global implications, environmental effects, and cause(s). Earth Planet. Sci. Lett. 297 (1–2), 298–305. http://dx.doi.org/10.1016/j.epsl.2010.06.031.

Cramer, B.S., Aubry, M.-P., Miller, K.G., Olsson, R.K., Wright, J.D., Kent, D.V., 1999. An exceptional chronologic, isotopic and clay mineralogic record of the latest Paleocene thermal maximum, Bass River, NJ, ODP 174 AX. Bull. Soc. Géol. Fr. 170 (6), 883–897.

Crouch, E.M., Dickens, G.R., Brinkhuis, H., Aubry, M.-P., Hollis, C.J., Rogers, K.M., Visscher, H., 2003. The *Apectodinium* acme and terrestrial discharge during the Paleocene–Eocene thermal maximum: new palynological, geochemical and calcareous nannoplankton observations at Tawanui, New Zealand. Palaeogeogr. Palaeoclimatol. Palaeoecol. 194 (4), 387–403. http://dx.doi.org/10.1016/S0031-0182(03), 00334-1.

Cruse, A.M., Lyons, T.W., 2004. Trace metal records of regional paleoenvironmental variability in Pennsylvanian (Upper Carboniferous) black shales. Chem. Geol. 206 (3–4), 319–345. http://dx.doi.org/10.1016/j.chemgeo.2003.12.010.

Curtis, C.D., 1990. Aspects of climatic influence on the clay mineralogy and geochemistry of soils, palaeosols and clastic sedimentary rocks. J. Geol. Soc. Lond. 147 (2), 351–357. http://dx.doi.org/10.1144/gsjgs.147.2.0351.

Dickens, G.R., 2001. Carbon addition and removal during the Late Palaeocene Thermal Maximum: basic theory with a preliminary treatment of the isotope record at ODP Site 1051, Blake Nose. Geol. Soc. Lond. Spec. Publ. 183, 293–305. http://dx.doi.org/10.1144/GSL.SP.2001.183.01.14.

Dickens, G.R., O'Neil, J.R., Rea, D.K., Owen, R.M., 1995. Dissociation of oceanic methane hydrate as a cause of the carbon isotope excursion at the end of the Paleocene. Paleoceanography 10 (6), 965–971. http://dx.doi.org/10.1029/95PA02087.

Dupuis, C., Aubry, M.-P., Steurbaut, E., Berggren, W.A., Ouda, K., Magioncalda, R., Cramer, B.S., Kent, D.V., Speijer, R.P., Heilmann-Clausen, C., 2003. The Dababiya Quarry section:

lithostratigraphy, clay mineralogy, geochemistry and paleontology. Micropaleontology 49 (s1), 41–59. http://dx.doi.org/10.2113/49.Suppl_1.41.
Dypvik, H., Harris, N.B., 2001. Geochemical facies analysis of fine-grained siliciclastics using Th/U, Zr/Rb and (Zr+Rb)/Sr ratios. Chem. Geol. 181 (1–4), 131–146. http://dx.doi.org/10.1016/S0009-2541(01), 00278-9.
Erbacher, J., Thurow, J., Littke, R., 1996. Evolution patterns of radiolaria and organic matter variations: a new approach to identify sea-level changes in mid-Cretaceous pelagic environments. Geology 24 (6), 499–502. http://dx.doi.org/10.1130/0091-7613(1996)024<0499:EPORAO>2.3.CO;2.
Ernst, S.R., Guasti, E., Dupuis, C., Speijer, R.P., 2006. Environmental perturbation in the southern Tethys across the Paleocene/Eocene boundary (Dababiya, Egypt): foraminiferal and clay mineral records. Mar. Micropaleontol. 60 (1), 89–111. http://dx.doi.org/10.1016/j.marmicro.2006.03.002.
Fischer, C., Schmidt, C., Bauer, A., Gaupp, R., Heide, K., 2009. Mineralogical and geochemical alteration of low-grade metamorphic black slates due to oxidative weathering. Chem. Erde Geochem. 69 (2), 127–142. http://dx.doi.org/10.1016/j.chemer.2009.02.002.
Gavrilov, Y.O., Shcherbinina, E.A., Oberhänsli, H., 2003. Paleocene–Eocene boundary events in the northeastern Peri-Tethys. Geol. Soc. Am. Spec. Pap. 369, 147–168. http://dx.doi.org/10.1130/0-8137-2369-8.147.
Gradstein, F.M., Ogg, J.G., Smith, A.G. (Eds.), 2004. A Geologic Time Scale. Cambridge University Press, Cambridge, United Kingdom (610 pp.).
Guasti, E., 2005. Early Paleogene environmental turnover in the southern Tethys as recorded by foraminiferal and organic-walled dinoflagellate cysts assemblages. PhD Thesis, Universität Bremen, Bremen, Germany, 203 pp.
Guasti, E., Speijer, R.P., Brinkhuis, H., Smit, J., Steurbaut, E., 2006. Paleoenvironmental change at the Danian-Selandian transition in Tunisia: foraminifera, organic-walled dinoflagellate cyst and calcareous nannofossil records. Mar. Micropaleontol. 59 (3–4), 210–229. http://dx.doi.org/10.1016/j.marmicro.2006.02.008.
Hedges, J.I., Clark, W.A., Cowie, G.L., 1988. Fluxes and reactivities of organic matter in a coastal marine bay. Limnol. Oceanogr. 33 (5), 1137–1152. http://dx.doi.org/10.4319/lo.1988.33.5.1137.
Higgins, J.A., Schrag, D.P., 2006. Beyond methane: towards a theory for the Paleocene–Eocene Thermal Maximum. Earth Planet. Sci. Lett. 245 (3–4), 523–537. http://dx.doi.org/10.1016/j.epsl.2006.03.009.
Jenkyns, H.C., 2010. Geochemistry of oceanic anoxic events. Geochem. Geophys. Geosyst. 11 (3), Q03004. http://dx.doi.org/10.1029/2009GC002788.
John, C.M., Bohaty, S.M., Zachos, J.C., Sluijs, A., Gibbs, S., Brinkhuis, H., Bralower, T.J., 2008. North American continental margin records of the Paleocene–Eocene thermal maximum: implications for global carbon and hydrological cycling. Paleoceanography 23, PA2217. http://dx.doi.org/10.1029/2007PA001465.
Jones, B., Manning, D.A.C., 1994. Comparison of geochemical indices used for the interpretation of paleoredox conditions in ancient mudstones. Chem. Geol. 111 (1–4), 111–129. http://dx.doi.org/10.1016/0009-2541(94)90085-X.
Katz, M.E., Pak, D.K., Dickens, G.R., Miller, K.G., 1999. The source and fate of massive carbon input during the Latest Paleocene Thermal Maximum. Science 286 (5444), 1531–1533. http://dx.doi.org/10.1126/science.286.5444.1531.
Kennett, J.P., Stott, L.D., 1991. Abrupt deep-sea warming, palaeoceanographic changes and benthic extinctions at the end of the Palaeocene. Nature 353, 225–229. http://dx.doi.org/10.1038/353225a0.
Knox, R.W.O.B., Aubry, M.P., Berggren, W.A., Dupuis, C., Ouda, K., Magioncalda, R., Soliman, M., 2003. The Qreiya section at Gebel Abu Had: lithostratigraphy, clay mineralogy, geochemistry and biostratigraphy. Micropaleontology 49 (s1), 93–104. http://dx.doi.org/10.2113/49.Suppl_1.93.
Kopp, R.E., Schumann, D., Raub, T.D., Powars, D.S., Godfrey, L.V., Swanson-Hysell, N.L., Maloof, A.C., Vali, H., 2009. An Appalachian Amazon? Magnetofossil evidence for the development of a tropical river-like system in the mid-Atlantic United States during the Paleocene–Eocene thermal maximum. Paleoceanography 24, PA4211. http://dx.doi.org/10.1029/2009PA001783.
Kraal, P., Slomp, C.P., Forster, A., Kuypers, M.M.M., 2010. Phosphorus cycling from the margin to abyssal depths in the proto-Atlantic during oceanic anoxic event 2. Palaeogeogr. Palaeoclimatol. Palaeoecol. 295 (1–2), 42–54. http://dx.doi.org/10.1016/j.palaeo.2010.05.014.
Küspert, W., 1982. Environmental change during oil shale deposition as deduced from stable isotope ratios. In: Einsele, S., Seilacher, A. (Eds.), Cyclic and Event Stratification. Springer, New York, USA, pp. 482–501.
Lavergren, U., Astrom, M.E., Bergback, B., Holmstrom, H., 2009. Mobility of trace elements in black shale assessed by leaching tests and sequential chemical extraction. Geochem. Explor. Environ. Anal. 9 (1), 71–79. http://dx.doi.org/10.1144/1467-7873/08-188.
Littke, R., Klussmann, U., Krooss, B., Leythaeuser, D., 1991. Quantification of loss of calcite, pyrite, and organic matter due to weathering of Toarcian black shales and effects on kerogen and bitumen characteristics. Geochim. Cosmochim. Acta 55 (11), 3369–3378. http://dx.doi.org/10.1016/0016-7037(91)90494-P.
Lourens, L.J., Sluijs, A., Kroon, D., Zachos, J.C., Thomas, E., Röhl, U., Bowles, J., Raffi, I., 2005. Astronomical pacing of late Palaeocene to early Eocene global warming events. Nature 435 (7045), 1083–1086. http://dx.doi.org/10.1038/nature03814.
Lüniger, G., Schwark, L., 2002. Characterisation of sedimentary organic matter by bulk and molecular geochemical proxies: an example from an Oligocene maar-type Lake Enspel, Germany. Sediment. Geol. 148 (1–2), 275–288. http://dx.doi.org/10.1016/S0037-0738(01), 00222-6.
Lyons, T.W., Severmann, S., 2006. A critical look at iron paleoredox proxies: new insights from modern euxinic marine basins. Geochim. Cosmochim. Acta 70 (23), 5698–5722. http://dx.doi.org/10.1016/j.gca.2006.08.021.
Magioncalda, R., Dupuis, C., Smith, T., Steurbaut, E., Gingerich, P.D., 2004. Paleocene–Eocene carbon isotope excursion in organic carbon and pedogenic carbonate: direct comparison in a continental stratigraphic section. Geology 32 (7), 553–556. http://dx.doi.org/10.1130/G20476.1.
Murphy, A.E., Sageman, B.B., Hollander, D.J., Lyons, T.W., Brett, C.E., 2000. Black shale deposition and faunal overturn in the Devonian Appalachian Basin: clastic starvation, seasonal water–column mixing, and efficient biolimiting nutrient recycling. Paleoceanography 15 (3), 280–291. http://dx.doi.org/10.1029/1999PA000445.
Nicolo, M.J., Dickens, G.R., Hollis, C.J., Zachos, J.C., 2007. Multiple early Eocene hyperthermals: their sedimentary expression on the New Zealand continental margin and in the deep sea. Geology 35 (8), 699–702. http://dx.doi.org/10.1130/G23648A.1.
Nicolo, M.J., Dickens, G.R., Hollis, C.J., 2010. South Pacific intermediate water oxygen depletion at the onset of the Paleocene–Eocene Thermal Maximum as depicted in New Zealand margin sections. Paleoceanography 25, PA4210. http://dx.doi.org/10.1029/2009PA001904.
Ouda, K., 2003. The Paleocene/Eocene boundary in Egypt: an overview. Micropaleontology 49 (s1), 15–40. http://dx.doi.org/10.2113/49.Suppl_1.15.
Paillard, D., 2001. Glacial cycles: toward a new paradigm. Rev. Geophys. 39 (3), 325–346. http://dx.doi.org/10.1029/2000RG000091.
Petrizzo, M.R., 2005. An early late Paleocene event on Shatsky Rise, northwest Pacific Ocean (ODP Leg 198): evidence from planktonic foraminiferal assemblages. In: Bralower, T.J., Premoli Silva, I., Malone, M.J. (Eds.), An early late Paleocene event on Shatsky Rise, northwest Pacific Ocean (ODP Leg 198): Evidence from planktonic foraminiferal assemblages: Proceedings of the Ocen Drilling Project, Scientific Results, 198, Ocean Drilling Program, College Station, Texas, pp. 1–29. http://dx.doi.org/10.2973/odp.proc.sr.198.102.2005.
Piper, D.Z., Calvert, S.E., 2009. A marine biogeochemical perspective on black shale deposition. Earth Sci. Rev. 95 (1–2), 63–96. http://dx.doi.org/10.1016/j.earscirev.2009.03.001.
Quillévéré, F., Norris, R.D., Kroon, D., Wilson, P.A., Wilson, P., 2008. Transient ocean warming and shifts in carbon reservoirs during the early Danian. Earth Planet. Sci. Lett. 265 (3–4), 600–615. http://dx.doi.org/10.1016/j.epsl.2007.10.040.
Rabalais, N.N., Turner, R.E., Scavia, D., 2002. Beyond science into policy: Gulf of Mexico hypoxia and the Mississippi River. BioScience 52 (2), 129–142. http://dx.doi.org/10.1641/0006-3568(2002) 052[0129:BSIPGO]2.0.CO;2.
Rabalais, N.N., Turner, R.E., Diaz, R.J., Justic, D., 2009. Global change and eutrophication of coastal waters. ICES J. Mar. Sci. 66 (7), 1528–1537. http://dx.doi.org/10.1093/icesjms/fsp047.
Rachold, V., Brumsack, H.J., 2001. Inorganic geochemistry of Albian sediments from the Lower Saxony Basin NW Germany: palaeoenvironmental constraints and orbital cycles. Palaeogeogr. Palaeoclimatol. Palaeoecol. 174 (1–3), 121–143. http://dx.doi.org/10.1016/S0031-0182(01), 00290-5.
Ravizza, G., Norris, R.N., Blusztajn, J., Aubry, M.P., 2001. An Osmium isotope excursion associated with the Late Paleocene Thermal Maximum: evidence of intensified chemical weathering. Paleoceanography 16 (2), 155–163. http://dx.doi.org/10.1029/2000PA000541.
Rimmer, S.M., 2004. Geochemical paleoredox indicators in Devonian–Mississippian black shales, Central Appalachian Basin (USA). Chem. Geol. 206 (3–4), 373–391. http://dx.doi.org/10.1016/j.chemgeo.2003.12.029.
Rimmer, S.M., Thompson, J.A., Goodnight, S.A., Robl, T.L., 2004. Multiple controls on the preservation of organic matter in Devonian–Mississippian marine black shales: geochemical and petrographic evidence. Palaeogeogr. Palaeoclimatol. Palaeoecol. 215 (1–2), 125–154. http://dx.doi.org/10.1016/j.palaeo.2004.09.001.
Sælen, G., Tyson, R.V., Telnæs, N., Talbot, M.R., 2000. Contrasting watermass conditions during deposition of the Whitby Mudstone (Lower Jurassic) and Kimmeridge Clay (Upper Jurassic) formations, UK. Palaeogeogr. Palaeoclimatol. Palaeoecol. 163 (3–4), 163–196. http://dx.doi.org/10.1016/S0031-0182(00), 00150-4.
Sageman, B.B., Murphy, A.E., Werne, J.P., Ver Straeten, C.A., Hollander, D.J., Lyons, T.W., 2003. A tale of shales: the relative roles of production, decomposition, and dilution in the accumulation of organic-rich strata, Middle–Upper Devonian, Appalachian basin. Chem. Geol. 195 (1–4), 229–373. http://dx.doi.org/10.1016/S0009-2541(02), 00397-2.
Salem, R., 1976. Evolution of Eocene–Miocene sedimentation patterns in parts of Northern Egypt. AAPG Bull. 60 (1), 34–64.
Schmitz, B., Pujalte, V., Núñez-Betelu, K., 2001. Climate and sea-level perturbations during the Incipient Eocene Thermal Maximum: evidence from siliciclastic units in the Basque Basin (Ermua, Zumaia and Trabakua Pass), northern Spain. Palaeogeogr. Palaeoclimatol. Palaeoecol. 165 (3–4), 299–320. http://dx.doi.org/10.1016/S0031-0182(00)00167-X.
Schulte, P., Scheibner, C., Speijer, R.P., 2011. Fluvial discharge and sea-level changes controlling black shale deposition during the Paleocene–Eocene Thermal Maximum in the Dababiya Quarry Section, Egypt. Chem. Geol. 285 (1–4), 167–183. http://dx.doi.org/10.1016/j.chemgeo.2011.04.004.
Schumann, D., Raub, T.D., Kopp, R.E., Guerquin-Kern, J.L., Wu, T.D., Rouiller, I., Smirnov, A.V., Sears, S.K., Lucken, U., Tikoo, S.M., Hesse, R., Kirschvink, J.L., Vali, H., 2008. Gigantism in unique biogenic magnetite at the Paleocene–Eocene Thermal Maximum. Proc. Natl. Acad. Sci. 105 (46), 17648–17653. http://dx.doi.org/10.1073/pnas.0803634105.
Slomp, C.P., Van Cappellen, P., 2007. The global marine phosphorus cycle: sensitivity to oceanic circulation. Biogeosciences 4 (2), 155–171. http://dx.doi.org/10.5194/bg-4-155-2007.
Sluijs, A., Schouten, S., Pagani, M., Woltering, M., Brinkhuis, H., Sinninghe, D.J.S., Dickens, G.R., Huber, M., Reichart, G.-J., Stein, R., Matthiessen, J., Lourens, L.J., Pedentchouk, N., Backman, J., Moran, K., 2006. Subtropical Arctic Ocean temperatures during the Palaeocene/Eocene thermal maximum. Nature 441 (7093), 610–613. http://dx.doi.org/10.1038/nature04668.
Sluijs, A., Bowen, G.J., Brinkhuis, H., Lourens, L.J., Thomas, E., 2007. The Palaeocene–Eocene Thermal Maximum super greenhouse: biotic and geochemical signatures, age models and mechanisms of global change. In: Williams, M., Haywood, A.M.,

Gregory, J., Schmidt, D.N. (Eds.), Deep Time Perspectives on Climate Change: Marrying the Signal from Computer Models and Biological Proxies: TMS Special Publications, London, 2, pp. 323–349.
Sluijs, A., Brinkhuis, H., Crouch, E.M., John, C.M., Handley, L., Munsterman, D., Bohaty, S.M., Zachos, J.C., Reichart, G.J., Schouten, S., Pancost, R.D., Damste, J.S.S., Welters, N.L.D., Lotter, A.F., Dickens, G.R., 2008. Eustatic variations during the Paleocene–Eocene greenhouse world. Paleoceanography 23 (4), PA4216. http://dx.doi.org/10.1029/2008PA001615.
Soliman, M.F., 2003. Chemostratigraphy of the Paleocene/Eocene (P/E) boundary sediments at Gabal-el-Qreiya, Nile Valley, Egypt.
Speijer, R.P., 2003. Danian-Selandian sea-level change and biotic excursion on the southern Tethyan margin (Egypt). In: Wing, S.L., Gingerich, P.D., Schmitz, B., Thomas, E. (Eds.), Causes and consequences of globally warm climates in the early Paleogene. Geol. Soc. Am. Spec. Pap. 369, 275–290. http://dx.doi.org/10.1130/0-8137-2369-8.275.
Speijer, R.P., Morsi, A.M.M., 2002. Ostracode turnover and sea-level changes associated with the Paleocene–Eocene thermal maximum. Geology 30 (1), 23–26. http://dx.doi.org/10.1130/0091-7613(2002) 030<0023:OTASLC>2.0.CO;2.
Speijer, R.P., Wagner, T., 2002. Sea-level changes and black shales associated with the late Paleocene thermal maximum: organic–geochemical and micropaleontologic evidence from the southern Tethyan margin (Egypt–Israel). In: Koeberl, C., MacLeod, K.G. (Eds.), Catastrophic events and mass extinctions: impacts and beyond. Geol. Soc. Am. Spec. Pap. 356, 533–549. http://dx.doi.org/10.1130/0-8137-2356-6.533.
Speijer, R.P., Schmitz, B., van der Zwaan, G.J., 1997. Benthic foraminiferal extinction and repopulation in response to latest Paleocene Tethyan anoxia. Geology 25 (8), 683–686. http://dx.doi.org/10.1130/0091-7613(1997) 025<0683:BFEARI>2.3.CO;2.
Speijer, R.P., Schmitz, B., Luger, P., 2000. Stratigraphy of late Paleocene events in the Middle East: implications for low- to middle-latitude successions and correlations. J. Geol. Soc. Lond. 157 (1), 37–47. http://dx.doi.org/10.1144/jgs.157.1.37.
Sprong, J., Speijer, R.P., Steurbaut, E., 2009. Biostratigraphy of the Danian/Selandian transition in the southern Tethys. special reference to the lowest occurrence of planktic foraminifera *Igorina albeari*. Geol. Acta 7 (1–2), 63–77. http://dx.doi.org/10.1344/105.000000271.
Sprong, J., Youssef, M.A., Bornemann, A., Schulte, P., Steurbaut, E., Stassen, P., Kouwenhoven, T.J., Speijer, R.P., 2011. Characterization of the Latest Danian Event at the southern Tethyan margin (Nile Basin, Egypt) by means of benthic foraminiferal assemblages. Mar. Micropaleontol. 30, 1–17.
Sprong, J., Kouwenhoven, T.J., Bornemann, A., Schulte, P., Stassen, P., Steurbaut, E., Youssef, M.A., Speijer, R.P., 2012. Characterization of the Latest Danian Event by means of benthic foraminiferal assemblages along a depth transect at the southern Tethyan margin (Nile Basin, Egypt). Mar. Micropaleontol. 86–87, 15–31 (0.1016/j.marmicro.2012.01.001).
Srodon, J., Drits, V.A., McCarty, D.K., Hsieh, J.C.C., Eberl, D.D., 2001. Quantitative X-ray diffraction analysis of clay-bearing rocks from random preparations. Clays Clay Miner. 49 (6), 514–528. http://dx.doi.org/10.1346/CCMN.2001.0490604.
Stap, L., Sluijs, A., Thomas, E., Lourens, L., 2009. Patterns and magnitude of deep sea carbonate dissolution during Eocene Thermal Maximum 2 and H2, Walvis Ridge, southeastern Atlantic Ocean. Paleoceanography 24, PA1211. http://dx.doi.org/10.1029/2008PA001655.
Steurbaut, E., Sztrákos, K., 2008. Danian/Selandian boundary criteria and North Sea Basin–Tethys correlations based on calcareous nannofossil and foraminiferal trends in SW France. Mar. Micropaleontol. 67 (1–2), 1–29. http://dx.doi.org/10.1016/j.marmicro.2007.08.004.
Svensen, H., Planke, S., Malthe-Sorenssen, A., Jamtveit, B., Myklebust, R., Rasmussen, E., Torfinn, Rey, S.S., 2004. Release of methane from a volcanic basin as a mechanism for initial Eocene global warming. Nature 429, 542–545. (http://dx.doi.org/10.1038/nature02566).
Thomas, E., 2007. Cenozoic mass extinctions in the deep sea: what perturbs the largest habitat on Earth? Geol. Soc. Am. Spec. Pap. 424, 1–23. http://dx.doi.org/10.1130/2007.2424(01.
Thomas, E., Shackleton, N.J., 1996. The Paleocene–Eocene benthic foraminiferal extinction and stable isotope anomalies. Geol. Soc. Lond. Spec. Publ. 101, 401. http://dx.doi.org/10.1144/GSL.SP.1996.101.01.20.
Thomas, E., Zachos, J.C., 2000. Was the late Paleocene thermal maximum a unique event? GFF 122 (1), 169–170. http://dx.doi.org/10.1080/11035890001221169.
Thomson, J., Jarvis, I., Green, D.R.H., Green, D.A., Clayton, T., 1998. Mobility and immobility of redox-sensitive elements in deep-sea turbidites during shallow burial. Geochim. Cosmochim. Acta 62 (4), 643–656. http://dx.doi.org/10.1016/S0016-7037(97), 00378-5.
Tissot, B.P., Welte, D.H., 1984. Petroleum Formation and Occurrence. Springer, Heidelberg, Germany. (699 pp.).
Torfstein, A., Winckler, G., Tripati, A., 2009. Productivity feedback did not terminate the Paleocene–Eocene Thermal Maximum (PETM). Clim. Past 6 (2), 265–272. http://dx.doi.org/10.5194/cp-6-265-2010.
Tribovillard, N., Algeo, T.J., Lyons, T., Riboulleau, A., 2006. Trace metals as paleoredox and paleoproductivity proxies: an update. Chem. Geol. 232 (1–2), 12–32. http://dx.doi.org/10.1016/j.chemgeo.2006.02.012.
Tyson, R.V., 1995. Sedimentary Organic Matter: Organic Facies and Palynofacies. Chapman and Hall, London, United Kingdom . (615 pp.).
Van Cappellen, P., Ingall, E.D., 1994. Benthic phosphorus regeneration, net primary production, and ocean anoxia: a model of the coupled marine biogeochemical cycles of carbon and phosphorus. Paleoceanography 9 (5), 677–692. http://dx.doi.org/10.1029/94PA01455.
Van Itterbeeck, J., Sprong, J., Dupuis, C., Speijer, R.P., Steurbaut, E., 2007. Danian/Selandian boundary stratigraphy, paleoenvironment and Ostracoda from Sidi Nasseur, Tunisia. Mar. Micropaleontol. 62 (4), 211–234. http://dx.doi.org/10.1016/j.marmicro.2006.08.006.
van Os, B., Middelburg, J.J., de Lange, G.J., 1995. Extensive degradation and fractionation of organic matter during subsurface weathering. Aquat. Geochem. 1 (3), 303–312. http://dx.doi.org/10.1007/BF00822494.
Westerhold, T., Röhl, U., Donner, B., McCarren, H., Zachos, J.C., 2011. A complete high-resolution Paleocene benthic stable isotope record for the central Pacific (ODP Site 1209). Paleoceanography 26, PA2216. http://dx.doi.org/10.1029/2010PA002092.
Wignall, P.B., Maynard, J.R., 1993. The sequence stratigraphy of transgressive black shales. In: Katz, B.J., Pratt, L.M. (Eds.), Source rocks in a sequence stratigraphic framework. Studies in Geology, 37. American Association of Petroleum Geologists, Tulsa, Oklahoma, pp. 35–47.
Youssef, M.M., 2003. Structural setting of central and south Egypt: an overview. Micropaleontology 49 (s1), 1–13. http://dx.doi.org/10.2113/49.Suppl_1.1.
Zachos, J.C., Pagani, M., Sloan, L.C., Thomas, E., Billups, K., 2001. Trends, rhythms, and aberrations in global climate 65 Ma to present. Science 292 (5517), 686–693. http://dx.doi.org/10.1126/science.1059412.
Zachos, J.C., Röhl, U., Schellenberg, S.A., Sluijs, A., Hodell, D.A., Kelly, D.C., Thomas, E., Nicolo, M., Raffi, I., Lourens, L.J., McCarren, H., Kroon, D., 2005. Rapid acidification of the ocean during the Paleocene–Eocene Thermal Maximum. Science 308 (5728), 1611–1615. http://dx.doi.org/10.1126/science.1109004.
Zachos, J.C., McCarren, H., Murphy, B., Röhl, U., Westerhold, T., 2010. Tempo and scale of late Paleocene and early Eocene carbon isotope cycles: implications for the origin of hyperthermals. Earth Planet. Sci. Lett. 299 (1–2), 242–249. http://dx.doi.org/10.1016/j.epsl.2010.09.004.